# Multi-span Horizontal Structures 13

**Abstract**

In this chapter, we discuss the role of analysis in the structural engineering process for multi-span horizontal structures such as bridges. Typical examples of a girder bridge, an arch bridge, and a cable-stayed bridge are shown in Fig. 13.1. Multi-span girders are actually variable depth horizontal beams. They are used extensively in medium span highway bridge systems. Arch and cable-stayed structures are efficient for spans ranging up to 1000 m.

Chapters 9 and 10 dealt with analysis methods for indeterminate structures. Some of the analytical results presented in those chapters are utilized here to estimate critical loading patterns. Most of the analysis effort required in the engineering process is related to determining the maximum values of bending moment, axial force, and shear corresponding to the typical bridge loadings. Establishing these values for indeterminate structures requires a considerable amount of computational effort. In what follows, we illustrate this computational process for different types of bridges such as continuous girder, arch, and cable-stayed schemes using a commercial structural analysis software system.

## 13.1 The Engineering Process for Girders

The objective of the structural engineering process for a beam is to define the physical makeup, i.e., the location of supports, the material, the shape and dimensions of the cross section, and special cross-section features such as steel reinforcement in the case of a reinforced concrete beam. Given the absolute maximum values of shear and moment at a particular location, the choice of material, and the general shape of the cross section, one determines the specific cross-sectional dimensions by applying numerical procedures specified by a design code. This phase of the engineering process is called design detailing. *We focus here on that aspect of the process associated with the determination of the "maximum" values of shear and moment*.


J.J. Connor, S. Faraji, *Fundamentals of Structural Engineering*,
DOI 10.1007/978-3-319-24331-3_13

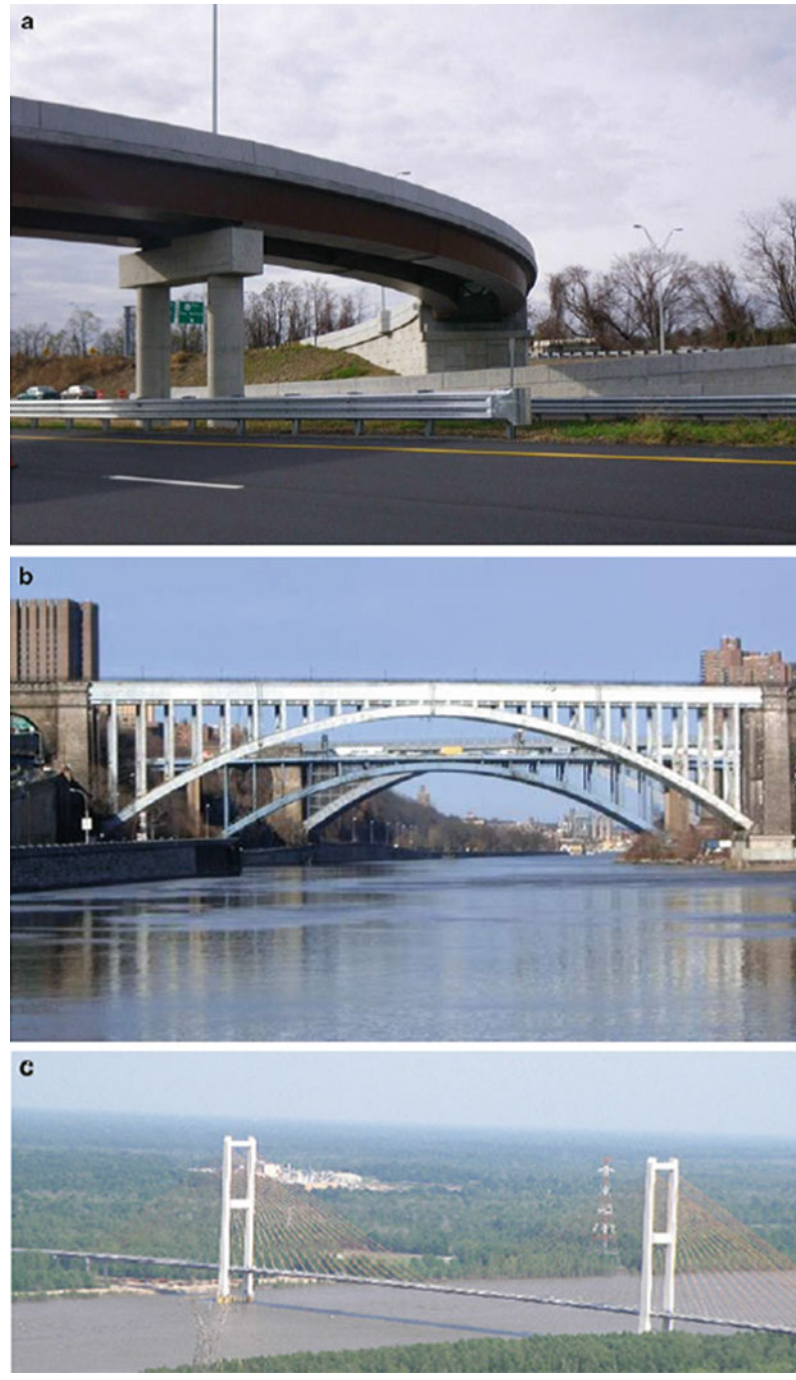


**Fig. 13.1** Bridge structures. (**a**) Multi-span girder bridge. (**b**) Arch bridge. (**c**) Cable stayed

In general, shear and bending moment result when an external loading is applied to a beam. Throughout the text, we have shown how one can establish the shear and moment distributions corresponding to a given loading. For statically determinate beams, the internal forces depend only on the external loading and geometry; they are independent of the cross-sectional properties. However, when the beam is indeterminate, such as a multi-span beam, the internal forces also depend on the

relative span lengths and cross-sectional properties. In this case, one needs to iterate on the geometry and properties in order to estimate the internal forces.

Now, the loading consists of two contributions: dead and live. The dead loading is fixed, i.e., its magnitude and spatial distribution are constant over time. Live loading is, by definition, time varying over the life of the structure. This variability poses a problem when we are trying to establish the maximum values of shear and moment. We need to consider a number of live load positions in order to identify the particular live load location that results in the absolute maximum values of shear and moment. One approach for multi-span beams is based on determining, for all positions of the live load, the absolute maximum value at sections along the span. Plots of global maxima at discrete sections along the span are called *force envelopes*.

It is important to distinguish between influence lines and force envelopes. An influence line relates a *force quantity at a particular point to the position of the live load*, *whereas a force envelope relates the absolute maximum value of the force quantity along the span*. We apply both approaches to establish design values.

## 13.2 Influence Lines for Indeterminate Beams Using Müller-Breslau's Principle

The topic of influence lines for statically determinate beams was introduced in Chap. 3. We include here a discussion of how one can generate influence lines for indeterminate beams using the Müller-Breslau principle [1]. We introduce the principle using the beam structure shown in Fig. 13.2a as an example. Later, in Chap. 15, we apply it to rigid frames.

Suppose one wants the influence line for *the negative moment at A* due to a downward vertical load. According to Müller-Breslau, one works with a modified structure obtained by inserting a moment release at A and applies a negative moment at A. The resulting structure is shown in Fig. 13.2b.

The deflected shapes of the modified structure due to a unit load applied at an arbitrary point, and a unit negative moment at A, are plotted in Fig. 13.2c, d. Since the beam is continuous at A, compatibility requires the net relative rotation at A to vanish. Then

$$\begin{aligned} &\theta_{\mathrm{Ax}} + \theta_{\mathrm{AA}} M_{\mathrm{A}} = 0 \\ &\Downarrow \\ &M_{\mathrm{A}} = -\frac{\theta_{\mathrm{Ax}}}{\theta_{\mathrm{AA}}} \end{aligned} \tag{13.1}$$

We note that $\theta_{\mathrm{Ax}} = \delta_{\mathrm{xA}}$ according to Maxwell's law of reciprocal displacements (see Sect. 9.2). Then (13.1) can be written as

$$M_{\mathrm{A}} = -\frac{\delta_{\mathrm{Ax}}}{\theta_{\mathrm{AA}}} \tag{13.2}$$

Since $\delta_{\mathrm{xA}}$ is at an arbitrary point, it follows that the *deflected shape of the modified structure due to a unit value of* $M_{\mathrm{A}}$ *is a scaled version of the influence line for* $M_{\mathrm{A}}$. The actual sense of $M_{\mathrm{A}}$ is determined by comparing the direction of the displacement with the direction of the applied load. In this example, the positive direction of the load is *downward*. We had applied a negative moment. Therefore, the sense of $M_{\mathrm{A}}$ needs to be reversed when the displacement is positive, in this case, download. The loading zones for the positive and negative values of $M_{\mathrm{A}}$ are shown in Fig. 13.3, which is based on the sign convention for moment, i.e., positive when compression on the upper fiber.

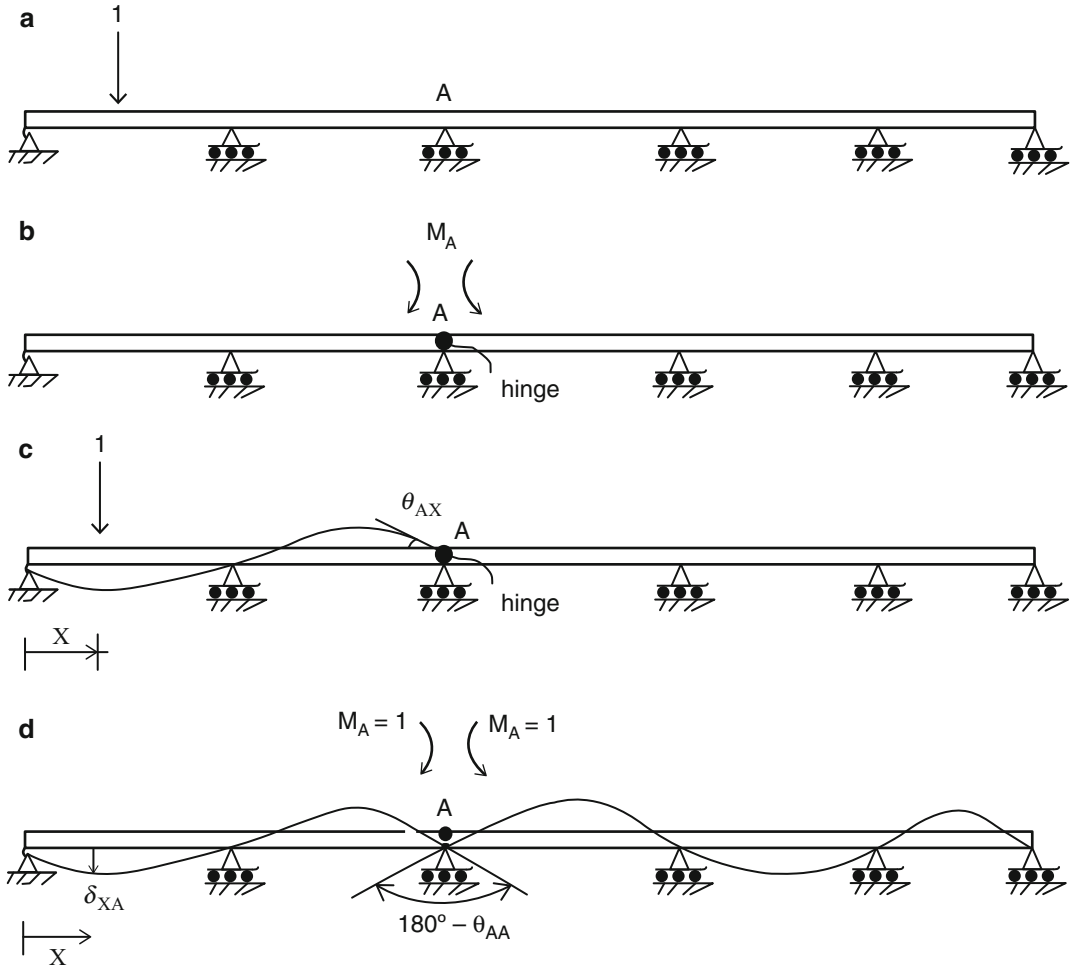


**Fig. 13.2** Application of Müller-Breslau principle (**a**) Example structure. (**b**) Negative moment. (**c**) Deflection due to load. (**d**) Deflection due to moment

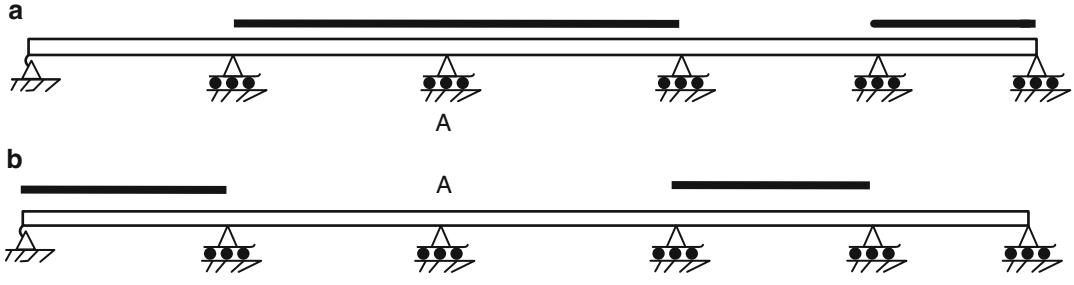


**Fig. 13.3** Loading zones for moment at A. (**a**) Negative moment at A. (**b**) Positive moment at A

We repeat this process to establish the influence line for the maximum positive moment at D, the center of span AC. The sequence of steps is illustrated in Fig. 13.4. Figure 13.5 defines the loading zones for positive and negative moments.

Summarizing the discussion presented above, the process of applying the Müller-Breslau principle to establish the influence line for a redundant force quantity involves the following steps:

1. Modify the actual structure by removing the restraint corresponding to the force quantity of interest.
2. Apply a unit value of the force quantity at the release and determine the deflected shape.
3. This deflected shape is a scaled version of the influence line. It consists of positive and negative zones for the force quantity. If the applied loading is a unit downward load, the positive zone includes those regions where the deflection is upward.

Since it is relatively easy to sketch deflected shapes, the Müller-Breslau principle allows one with minimal effort to establish the critical loading pattern for a redundant force quantity.

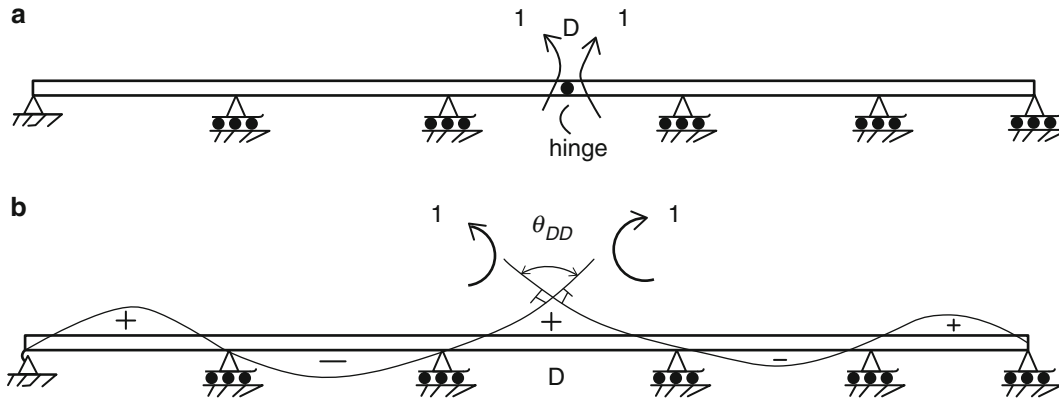


**Fig. 13.4** Modified structure and deflected shape for positive moment at D

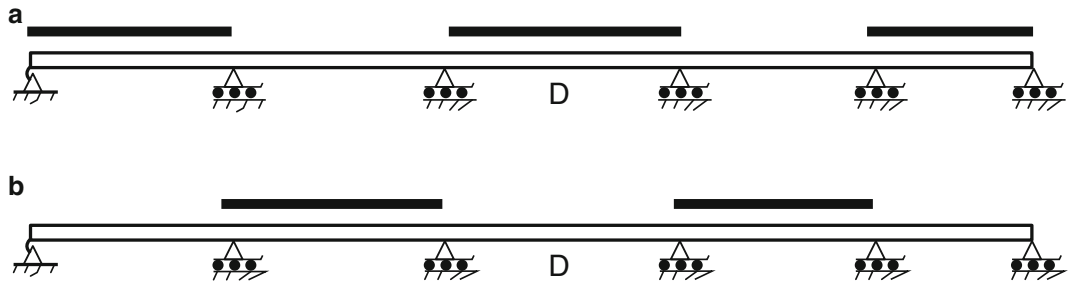


**Fig. 13.5** Loading zones for moment at D. (**a**) Positive value. (**b**) Negative value

*Example 13.1* Application of Müller-Breslau Principle

**Given:** The four-span beam shown in Fig. E13.1a.

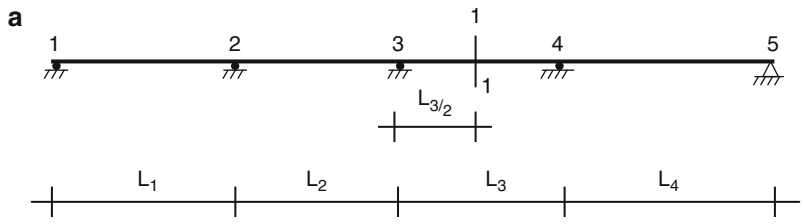


**Fig. E13.1a**

**Determine**: The influence lines for the upward vertical reaction at support 3 ($R_3$), the negative moment at support 3 ($M_3$), the positive moment at section 1-1 ($M_{1-1}$), and shear at section 1-1 ($V_{1-1}$). Also determine the critical loading patterns for a uniformly distributed load that produce the maximum values of $R_3$, $M_3$, $M_{1-1}$, and $V_{1-1}$.

**Solution**: The deflected shapes and influence lines for a unit downward load are plotted below.

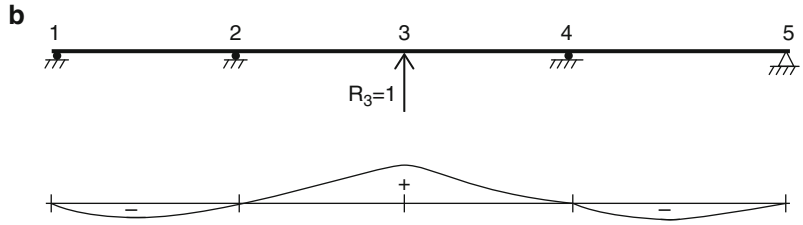


**Fig. E13.1b** Influence line for $R_3$

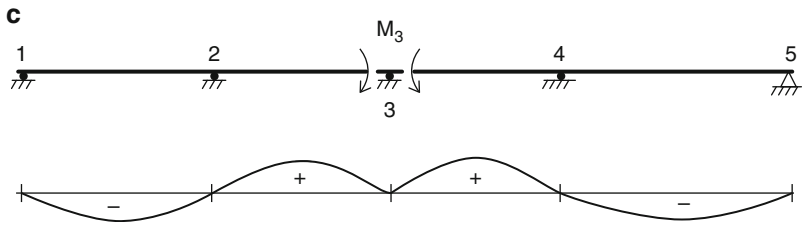


**Fig. E13.1c** Influence line for $M_3$

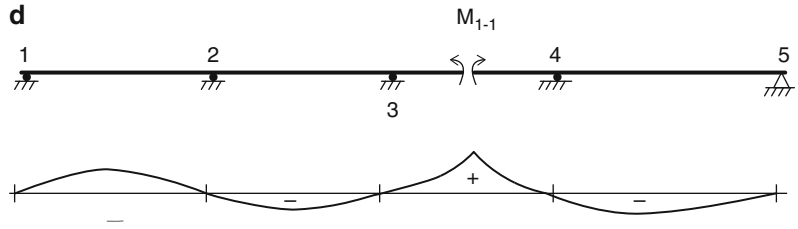


**Fig. E13.1d** Influence line for $M_{1-1}$

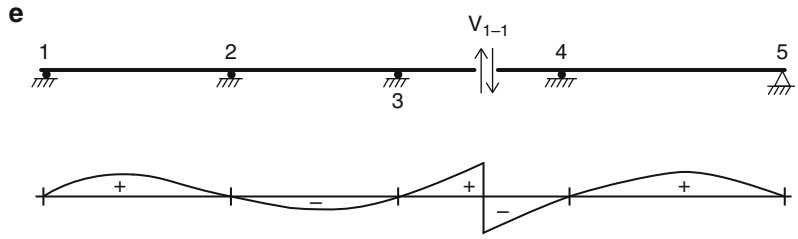


**Fig. E13.1e** Influence line for $V_{1-1}$

Loading patterns that produce the peak positive and negative values of these force parameters are shown in Figs. E13.1f, E13.1g, E13.1h, and E13.1i.

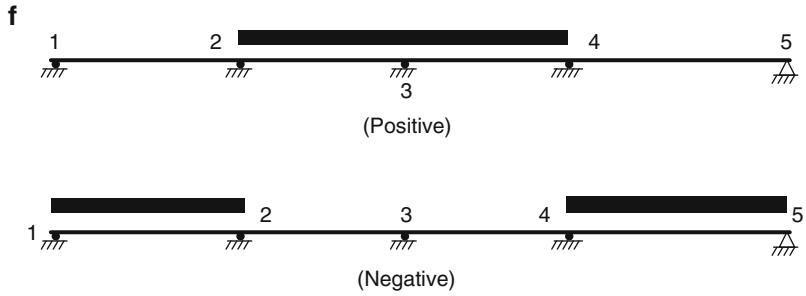


**Fig. E13.1f** Loading patterns for absolute maximum $R_3$

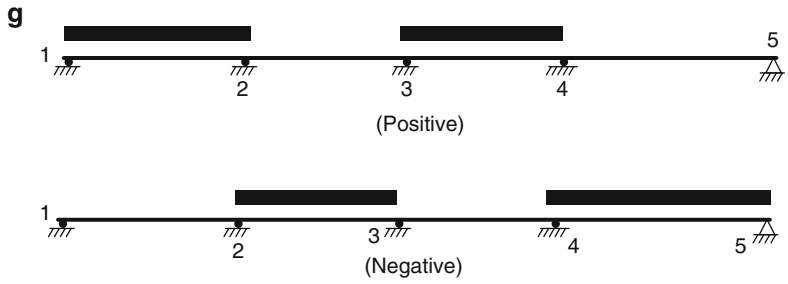


**Fig. E13.1g** Loading patterns for absolute maximum $M_{1-1}$

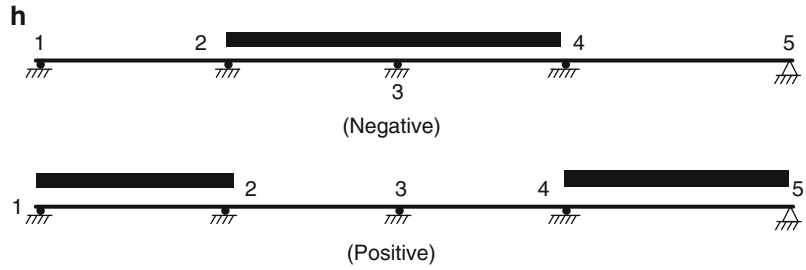


**Fig. E13.1h** Loading patterns for absolute maximum $M_3$

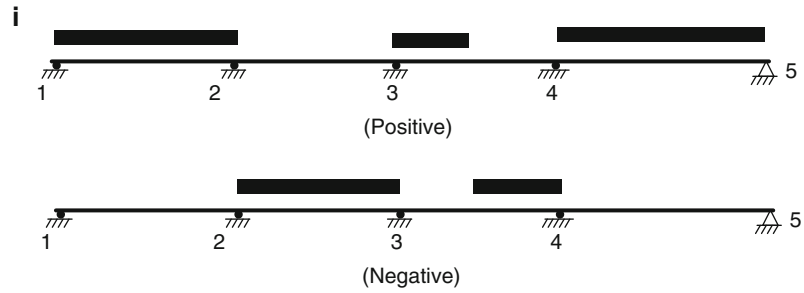


**Fig. E13.1i** Loading patterns for absolute maximum $V_{1-1}$

## 13.3 Engineering Issues for Multi-span Girder Bridges

### 13.3.1 Geometric Configurations

The superstructure of a typical highway girder bridge consists of longitudinal girders which support a concrete deck. The girders may be fabricated from either steel or concrete. The substructure is composed of piers and abutments which are founded on either shallow foundations or piles. In general, the makeup of the substructure depends on the soil conditions at the site. Bearings are employed to connect the girders to the substructure.

Bridge spans are classified as either short, medium, or long according to the total span length. Typical categories are

$$\begin{aligned} &\text{Short}: \ \text{less than } 125 \text{ ft } (38 \text{ m}) \\ &\text{Medium}: \ 125 - 400 \text{ ft } (38 - 120 \text{ m}) \\ &\text{Long}: \ \text{over } 400 \text{ ft } (120 \text{ m}) \end{aligned}$$

Typical highway bridge structural systems are composed of continuous beams. One could replace the continuous beam with an arrangement of simply supported beams. However, this choice requires additional bearings and introduces discontinuities in the deck slab at the interior supports that creates a serious problem since it provides a pathway for moisture and leads to corrosion of the bearings at the supports. Using a continuous beam allows one to achieve continuity of the deck slab and also eliminates some bearings. It is the preferred structural scheme for new bridges. Typical span arrangements are shown in Fig. 13.6. The current trend is to use a constant girder cross section throughout the span.

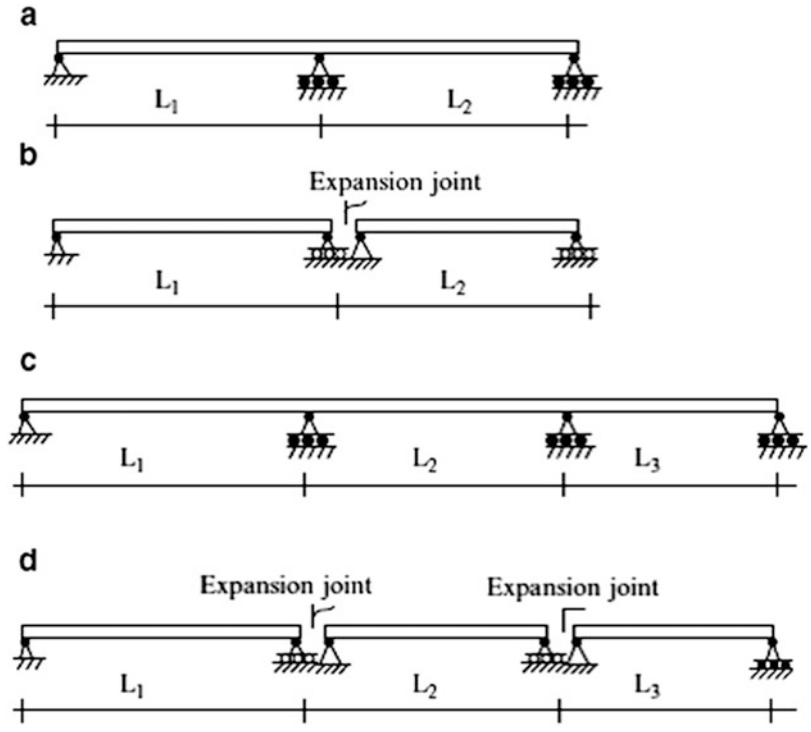


**Fig. 13.6** Span arrangements for multi-span beams. (**a**) Two spans continuous. (**b**) Two spans simply supported. (**c**) Three spans continuous. (**d**) Three spans simply supported

Historically, girder bridges were configured as a collection of single spans. This scheme is illustrated in Fig. 13.7a. In order to deal with longer interior spans, the cantilever scheme shown in Fig. 13.7b was introduced. Both schemes involve discontinuities in the girder/deck which provide pathways for moisture and lead to deterioration. To eliminate the interior discontinuities, the obvious option is to use a continuous girder as shown in Fig. 13.7c. We demonstrated in Chap. 9 that continuous beams are more efficient structurally, i.e., the peak internal forces are less than the corresponding forces for the simply supported case. Therefore, the required cross section tends to be lighter.

Even when a continuous girder is used, there still remains the problem of the discontinuities at the end supports (abutments). The problem is solved by using the scheme shown in Fig. 13.8. The abutments walls are supported on flexible piles that are rigidly connected to the deck/girder system. This concept is called an "integral abutment bridge." Since the abutment is rigidly attached to the deck/girder, a temperature change of the deck produces a longitudinal displacement of the abutment wall. In order to minimize the effect of the resulting lateral force, the abutments are supported on flexible piles and loose granular backfill is placed behind the wall. The longitudinal displacement due to temperature varies linearly with the span length, and consequently, the maximum span length is limited by the seasonal temperature change.

We generate an idealized model by replacing the action of the soil and piles with equivalent springs [2]. Figure 13.9a illustrates this approach. An estimate of the effect of support stiffness is obtained using the model shown in Fig. 13.9b.

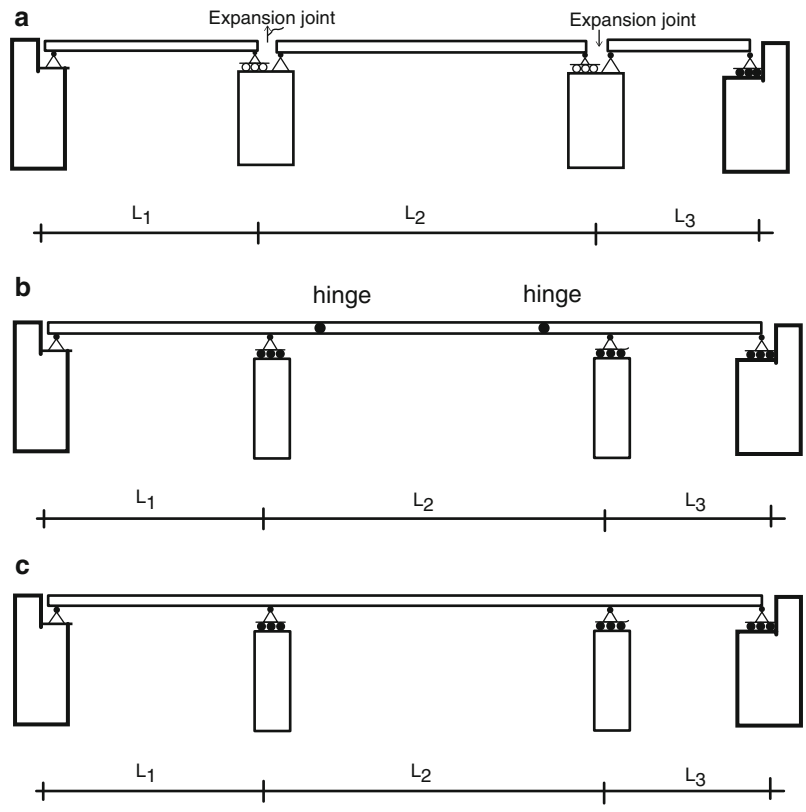


**Fig. 13.7** Multi-span bridge schemes (**a**) Simple spans. (**b**) Cantilever spans. (**c**) Continuous spans

### 13.3.2 Choice of Span Lengths

Given some overall crossing length, one needs to decide on the number and relative magnitude of the spans to be used to achieve the crossing. We utilize here some of the analytical results for multi-span continuous beams with constant $I$ subject to uniform loading generated in Chaps. 9 and 10. Figure 13.10 shows how the maximum moment varies with increasing number of spans. Note that there is a significant reduction in peak moment as the number of spans is increased, for a *given overall length*. Note also that the bending moment distribution for constant $I$ is independent of the value of $I$.

In general, for constant $I$, the bending moment distribution depends on the ratio of the span lengths. For the symmetrical case shown in Fig. 13.11, the analytical solution for the negative moment at an interior support has the form (see Example 10.5)

$$M^{-}_{\max} = g\left(\frac{L_2}{L_1}\right)\frac{wL_1^2}{8} \tag{13.3}$$

where

$$g\left(\frac{L_2}{L_1}\right) = \frac{1 + (L_2/L_1)^2}{1 + (3/2)(L_2/L_1)}$$

We express $L_1$ and $L_2$ as

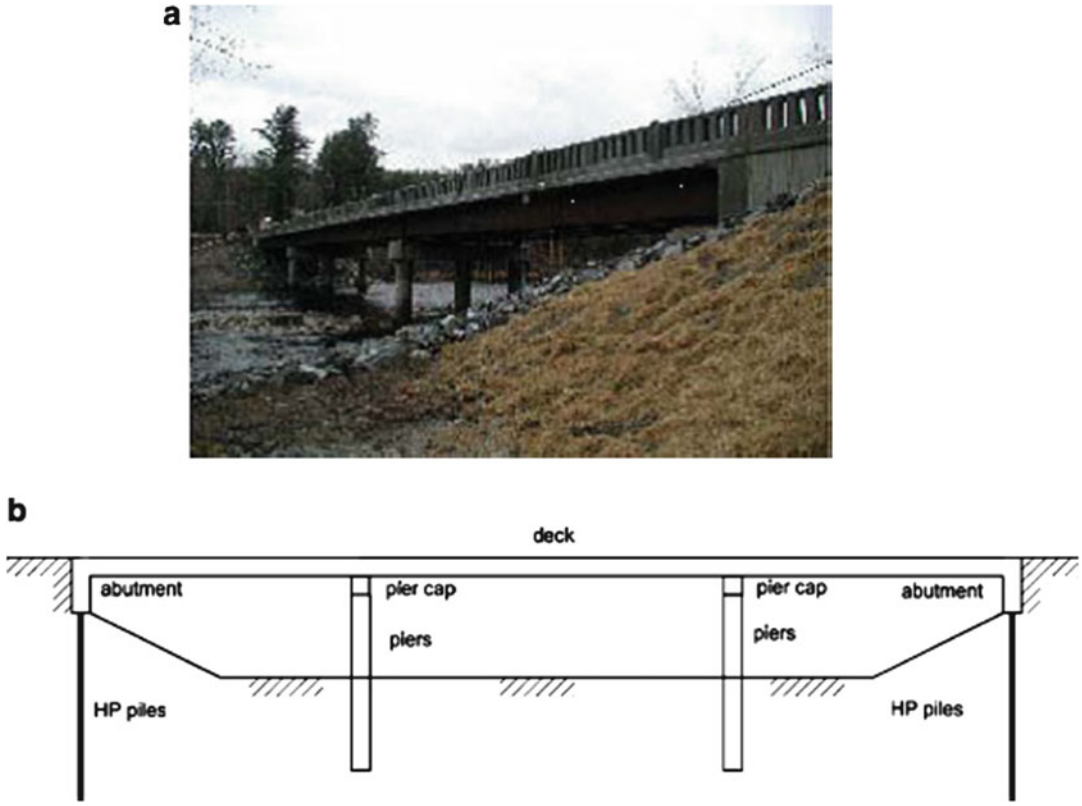


**Fig. 13.8** (**a**) Three-span integral abutment bridge in Orange, Massachusetts. (**b**) Elevation—three-span integral abutment bridge

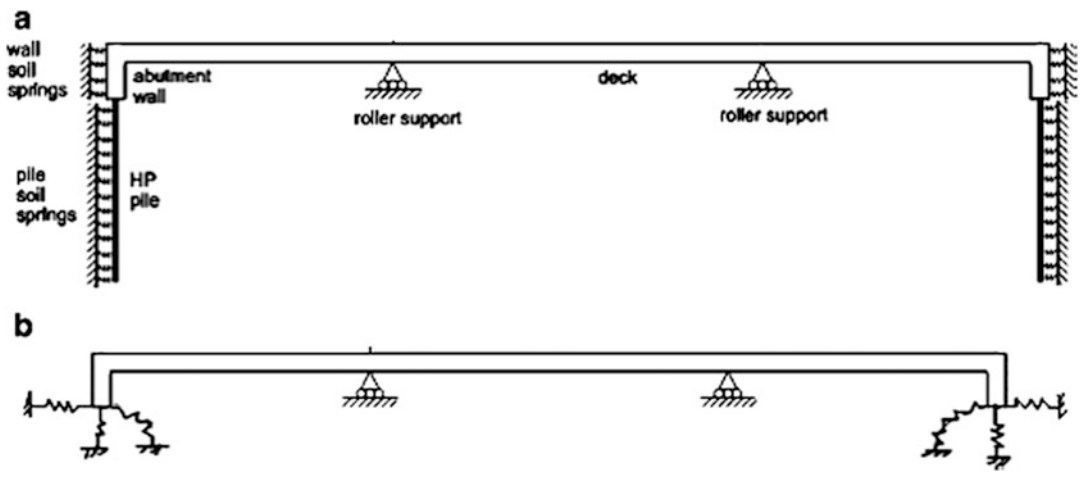


**Fig. 13.9** Idealized models for an integral abutment bridge (**a**) Global model. (**b**) Simplified model

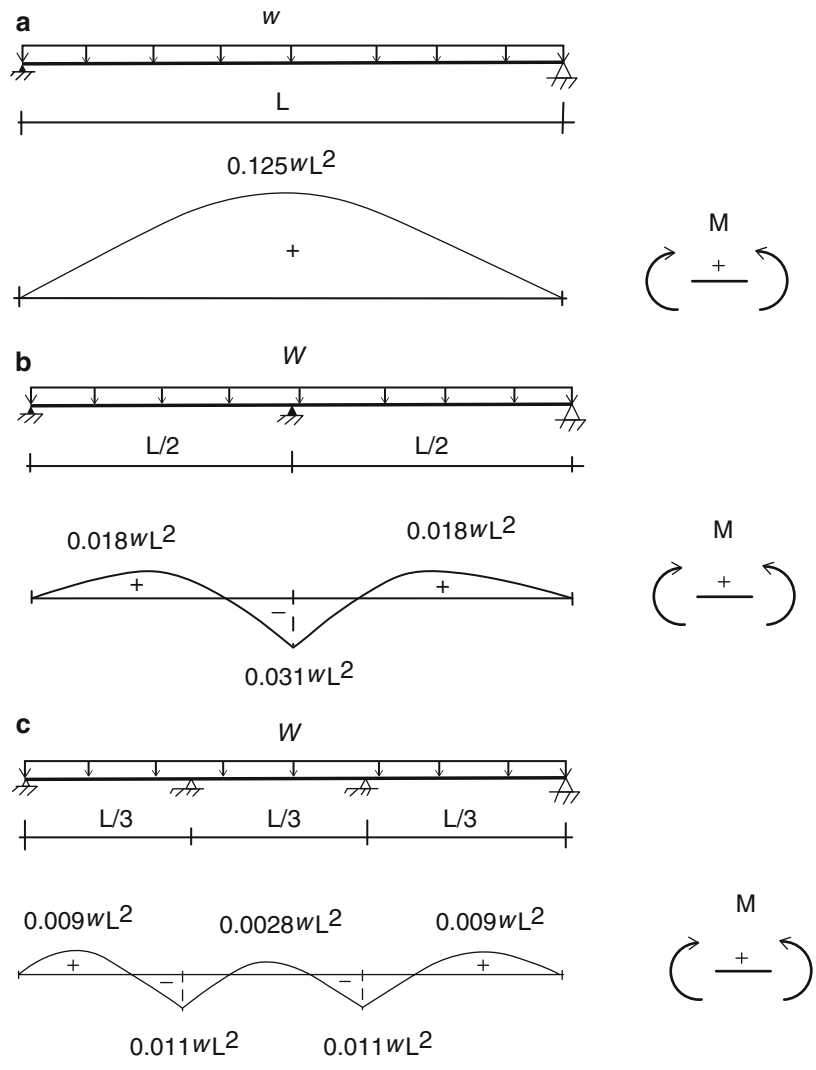


**Fig. 13.10** Variation of the bending moment distribution. (**a**) Simply supported. (**b**) Two-span scheme. (**c**) Three-span scheme

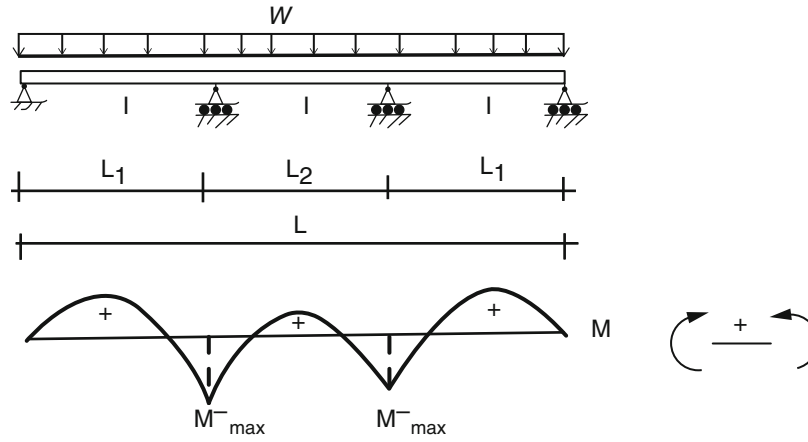


**Fig. 13.11** Bending moment distribution—three-span symmetrical scheme

$$L_2 = \alpha L$$
$$L_1 = \frac{(1-\alpha)L}{2} \tag{13.4}$$

With this notation, (13.3) expands to

$$M^-_{\max} = \frac{wL^2}{8} f(\alpha)$$
$$f(\alpha) = \frac{1 - 3\alpha + 7\alpha^2 - 5\alpha^3}{4(1+2\alpha)} \tag{13.5}$$

The variation of $f$ with $\alpha$ is plotted below.

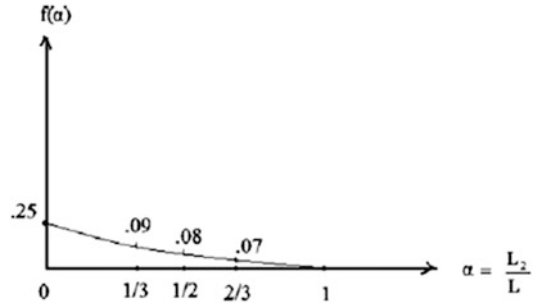


Taking $L_2 = L_1$ corresponds to $\alpha = 1/3$. The more common case is where α is between 1/3 and 1/2. When spans $L_1$ and $L_2$ are chosen, one applies the uniformly distributed loading and determines the peak value of negative moment using (13.5).

### 13.3.3 Live Loads for Multi-span Highway Bridge Girders: Moment Envelopes

The live load for a highway bridge is assumed to consist of two components: a uniform loading intended to simulate small vehicles, such as cars, and a set of concentrated loads that characterize heavy vehicles, such as trucks.

#### 13.3.3.1 Set of Concentrated Live Loads

The action of a heavy vehicle traveling across the total span is simulated by positioning a set of concentrated loads at various locations along the span. The load magnitude and axle spacing vary depending on the code that governs the design. For each load position, we determine the bending moment at specific points along the span. When the beam is statically determinate, it is possible to develop an analytical solution for the peak moment. This approach is described in Chap. 3. However, when the beam is indeterminate, one must resort to a numerical procedure. This approach is illustrated in Fig. 13.12. In practice, one first discretizes the spans and then positions the load at the individual discrete points. Assuming there are $n$ discrete points, one needs to carry out $n$ analyses. This results in $n$ bending moment distributions. At each discrete point, we determine the maximum positive and negative values from the set of $n$ values generated by the $n$ analyses. Finally, we construct a plot showing the "maximum" values of moment at each discrete point. This plot allows one to readily identify the absolute "maximum" moment by scanning over the plot. Since the values at each discrete point represent the *peak values at the point for all positions of the loading*, we interpret the plot as a *moment envelope*. Working with a refined span discretization provides detailed

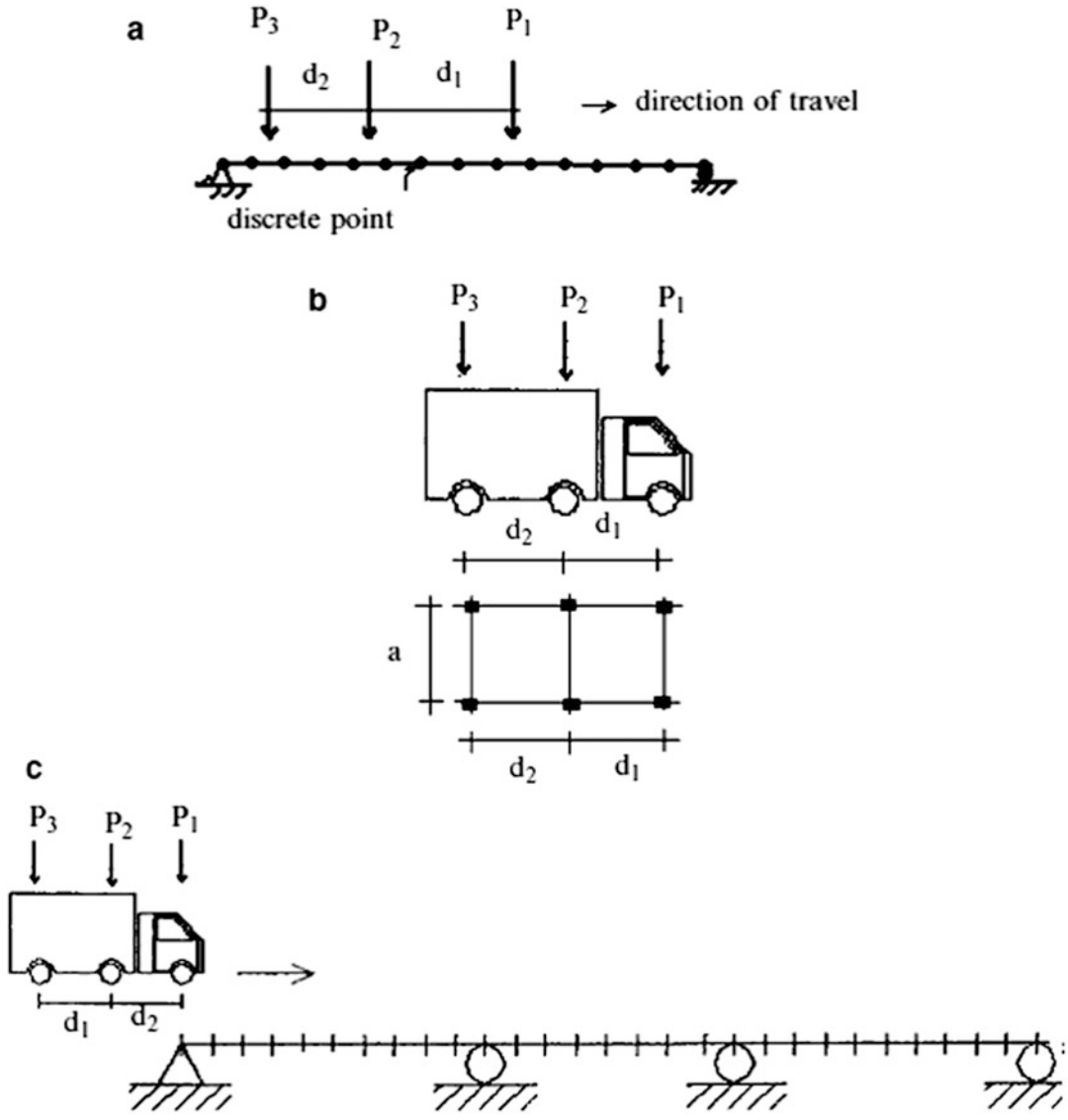


**Fig. 13.12** Truck loading and span discretization. (**a**) Span discretization. (**b**) Three-axle truck. (**c**) Multi-span discretization

information on the absolute shear and moment distributions. For example, 30 separate analyses are required to generate the moment envelope for the span discretization shown in Fig. 13.12c. We discuss next how one establishes the magnitudes of the concentrated loads.

#### 13.3.3.2 Transverse Distribution of Truck Load to Stringers

Figure 13.13 shows typical slab stringer highway bridge cross sections. The roadway is supported by a reinforced concrete slab, which rests on a set of longitudinal beams, called stringers. The stringers may be either steel sections or concrete elements.

In order to determine the truck load applied to the stringer, we position the truck such that one set of wheels is directly on the stringer. Figure 13.14 illustrates this case. *Note that P is the axle load.*

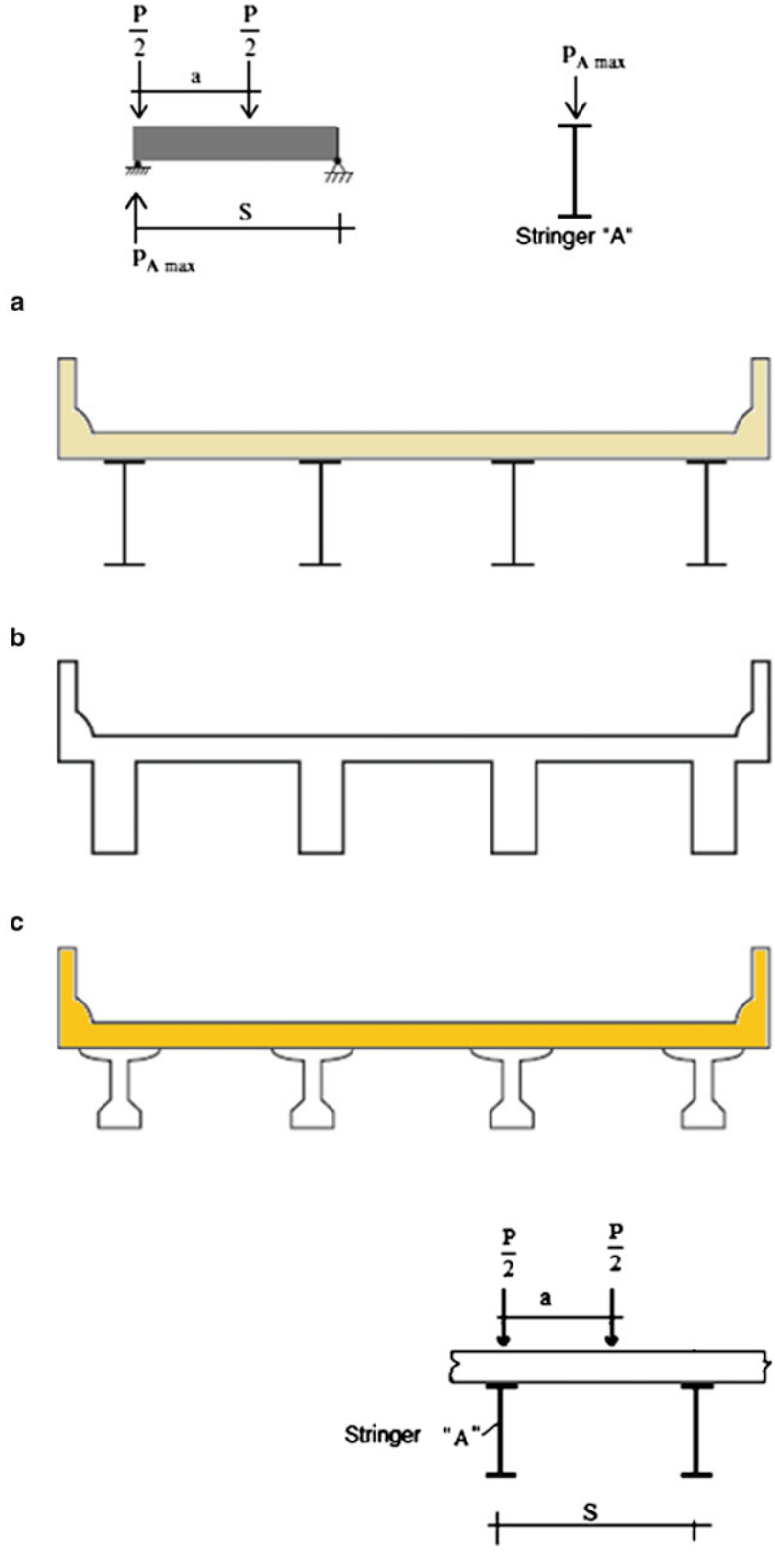


**Fig. 13.13** Typical slab-stringer bridge deck cross sections (**a**) Steel girders. (**b**) Concrete T beams. (**c**) Precast concrete beams




**Fig. 13.14** Transverse position of vehicle wheel loads

We assume the slab acts as a simply supported beam spanning between the stringers. This assumption is conservative. Then the load on stringer "A" is

$$P_{\text{Amax}} = \frac{P}{2} + \frac{P}{2}\left(\frac{S-a}{S}\right) = \frac{P}{2}\left(2 - \frac{a}{S}\right)$$

The axle distribution factor is defined as

$$\text{DF} = \frac{1}{2}\left(2 - \frac{a}{S}\right) \tag{13.6}$$

Using this definition, the load on the stringer is represented as

$$P_{\text{Amax}} = P(\text{DF})$$

Taking $S = 8$ ft and $a = 6$ ft yields $P_{\text{A max}} \approx 0.625P$

Another effect that needs to be included is impact. The loading is applied rapidly as the vehicle travels onto the bridge. A measure of the loading duration is the ratio of span length to vehicle velocity. When a loading is applied suddenly and maintained constant, the effect on the response of a structure is equivalent to the application of a static load whose magnitude is equal to twice the actual load. The concept of an impact factor is introduced to handle this effect. Intuitively, one would expect this factor to be larger for short spans, i.e., to vary inversely with span length. An impact magnification factor ($I$) of 30 % is commonly used. With this notation, the load on the stringer is given by

$$P_{i\ \text{design}} = P_i(1 + I)\text{DF} \tag{13.7}$$

where $P_i$ is the axle load.

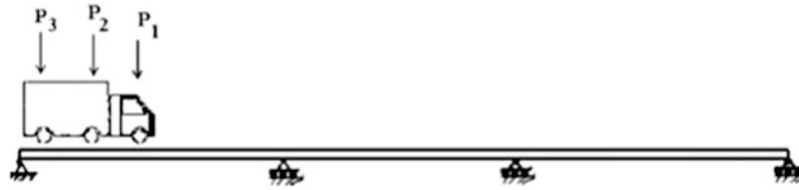


#### 13.3.3.3 Uniform Live Load

Small vehicles are modeled as a uniform loading applied selectively to individual spans. The purpose of this loading is to simulate the case where a set of passenger cars is stalled in a lane on one or more spans. *One uses the influence lines for the moments at mid-span and the interior supports to establish the loading patterns for lane loads*. The loading patterns for a three-span system are listed in Fig. 13.15c, d. Loading cases 1 and 2 produce the peak positive moment at the midpoint of the interior span; cases 3 and 4 generate the peak negative moment at the interior supports.

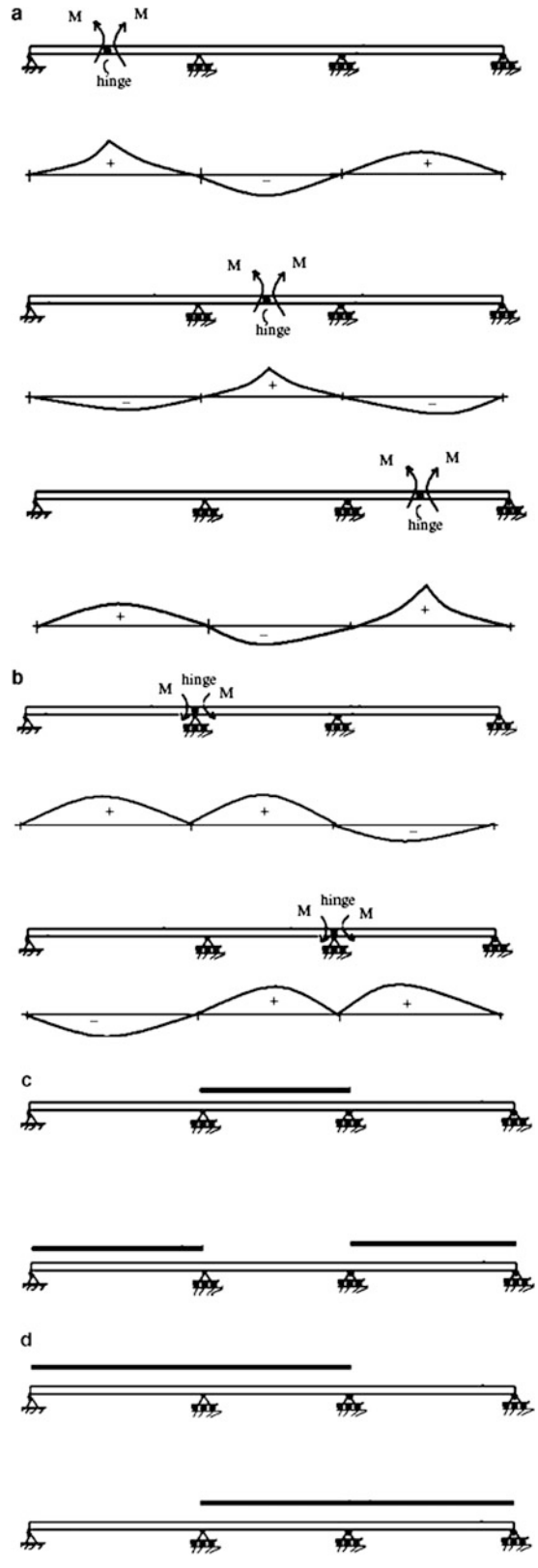


**Fig. 13.15** Lane load cases—loading patterns. (**a**) Influence lines for positive moments at mid-spans. (**b**) Influence lines for negative moments at the supports. (**c**) Maximum positive moment at mid-spans (cases 1 and 2). (**d**) Max negative moments at the supports (cases 3 and 4)

Given the loading patterns, one generates the bending moment distribution for each loading condition and then establishes the maximum values of the positive and negative moments at the *same discrete locations* selected for the truck loading. These results define the discrete moment envelope for the structure. Four separate analyses (cases 1–4) are required to construct the discrete moment envelope corresponding to the lane loading for this three-span example.

### 13.3.4 Loading Due to Support Settlements

In addition to the gravity loading associated with the weight of the beam and vehicles, one also needs to consider the moments induced in the structure due to support settlement. This calculation is relatively straightforward. The analytical solutions for two- and three-span symmetrical beams are generated in Examples 10.2 and 10.5. We list those results in Fig. 13.16 for convenience. Note that the peak moments are linear functions of $EI$. Note that the peak moment varies as $1/L^2$. Therefore support settlement is more significant for short spans vs. long spans.

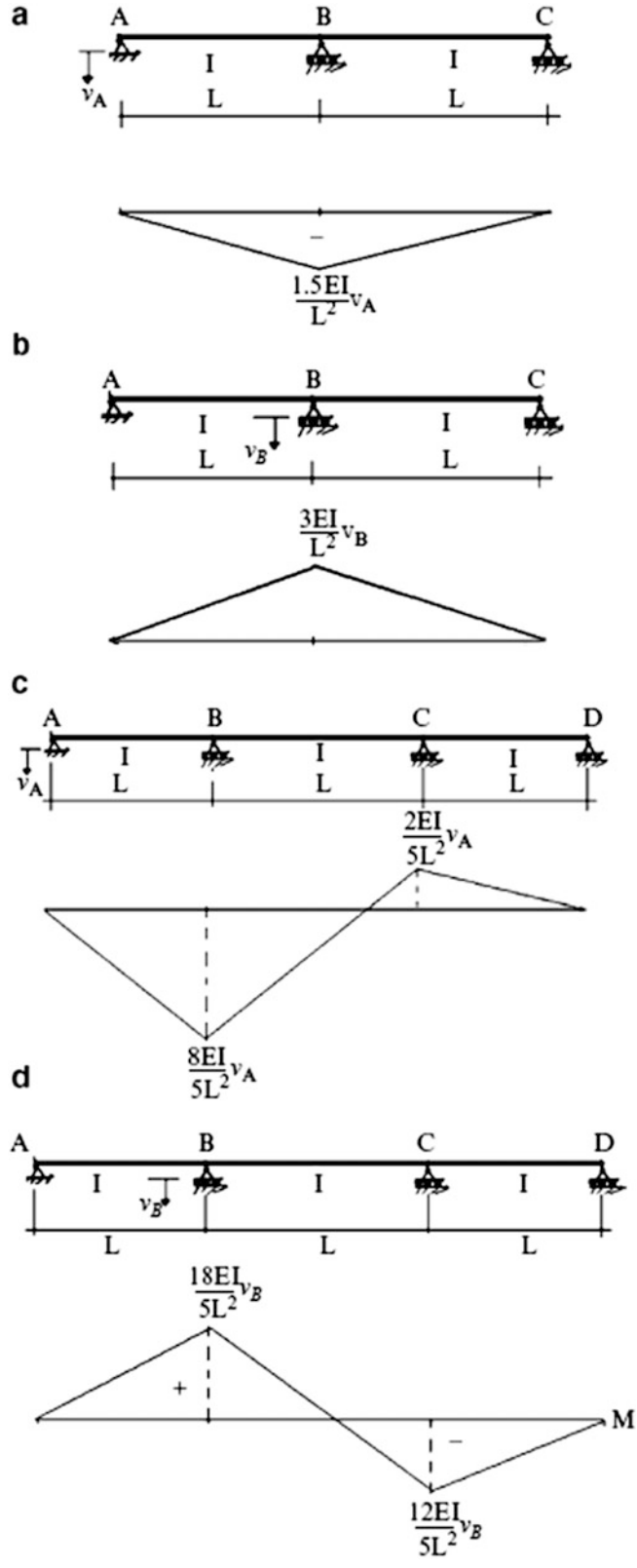


**Fig. 13.16** Moments due to support settlements. (**a**) Two-span case for $v_A$. (**b**) Two-span case for $v_B$. (**c**) Three-span case for $v_A$. (**d**) Three-span case for $v_B$

*Example 13.2:* Effect of Span Length on Support Settlement

**Given:** The three-span beam shown in Fig. E13.2a. The beam properties are $E = 200$ GPa and $I = 9000(10)^6$ mm$^4$.

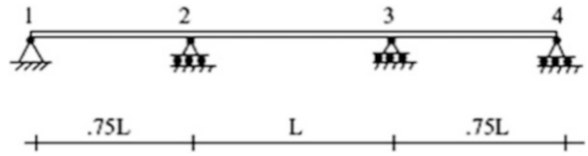


**Fig. E13.2a**

**Determine**: The bending moment distribution due to support settlement of 25 mm at supports A and B. Consider the following cases: (a) $L = 10$ m, (b) $L = 20$ m

**Solution**: The resulting moments are plotted in Figs. E13.2b and E13.2c. These results demonstrate that the effect of support settlement is more critical for the shorter span [case (a)].

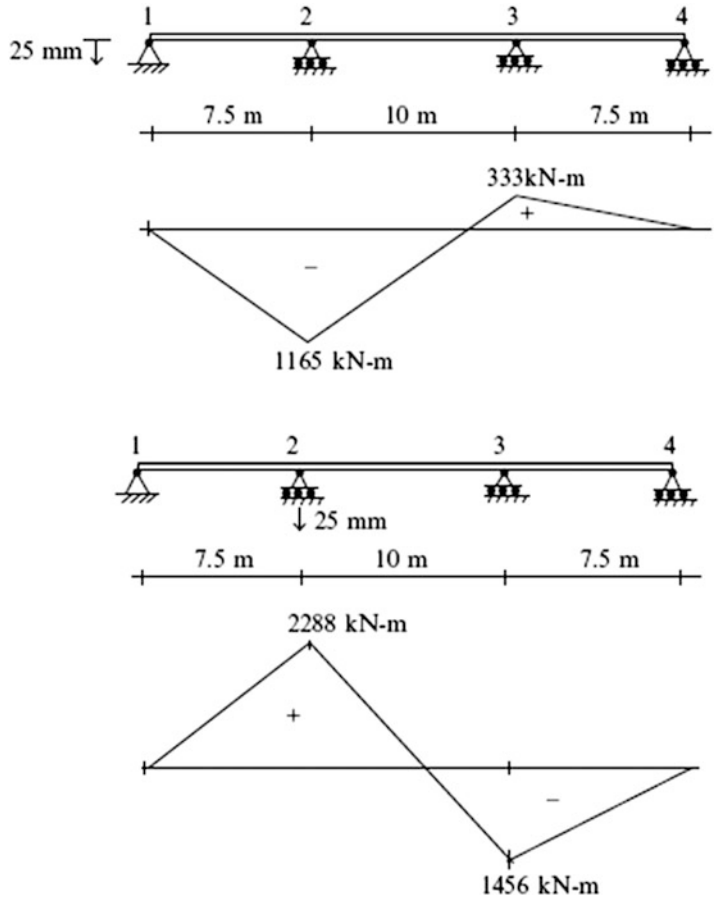


**Fig. E13.2b** Case a results

Case a: $L = 10$ m

Case b: $L = 20$ m

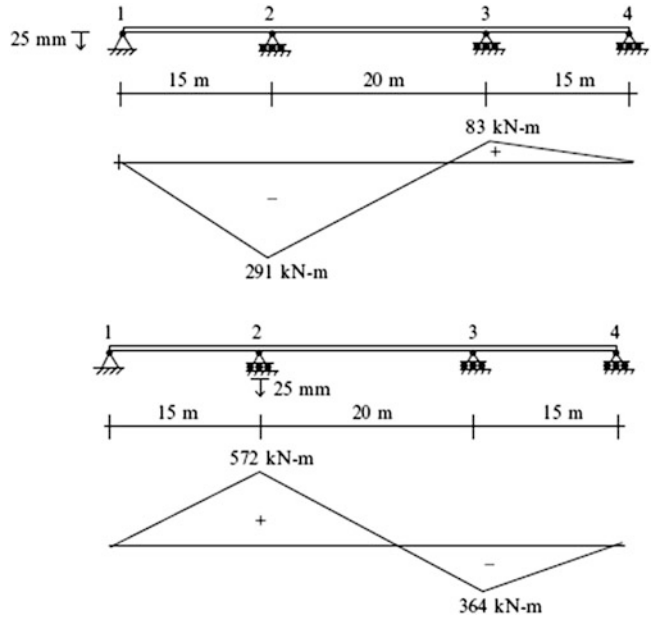


**Fig. E13.2c** Case b results

## 13.4 Case Studies

### 13.4.1 Case Study I: A Three-Span Continuous Girder Bridge

We illustrate the process of establishing design values using an actual bridge as a case study. The bridge is a three-span continuous girder bridge, with spans measuring 80 ft, 110 ft, and with an overall length of 270 ft. The superstructure consists of an 8 in. thick concrete slab acting in composite with four lines of steel girders spaced at 8.67 ft on center. The girder cross section is constant throughout the length. The deck carries two traffic lanes, continuous over the entire length of the bridge. The bearings are either hinge or roller supports. Figures 13.17 and 13.18 show the makeup of the bridge system and the details of the cross section. The bridge is modeled using an equivalent section equal to approximately one-fourth of the cross section of the bridge (one girder plus a 8.67 ft slab). Figure 13.18b defines the model used for this analysis.

*Our objectives are*

1. To determine the moment envelopes for truck and lane loading corresponding to a live uniform lane loading of 0.64 kip/ft and the truck loading defined in Fig. 13.19.

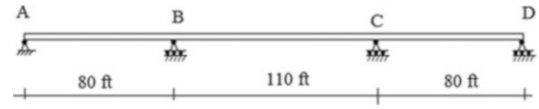


**Fig. 13.17** Girder bridge system

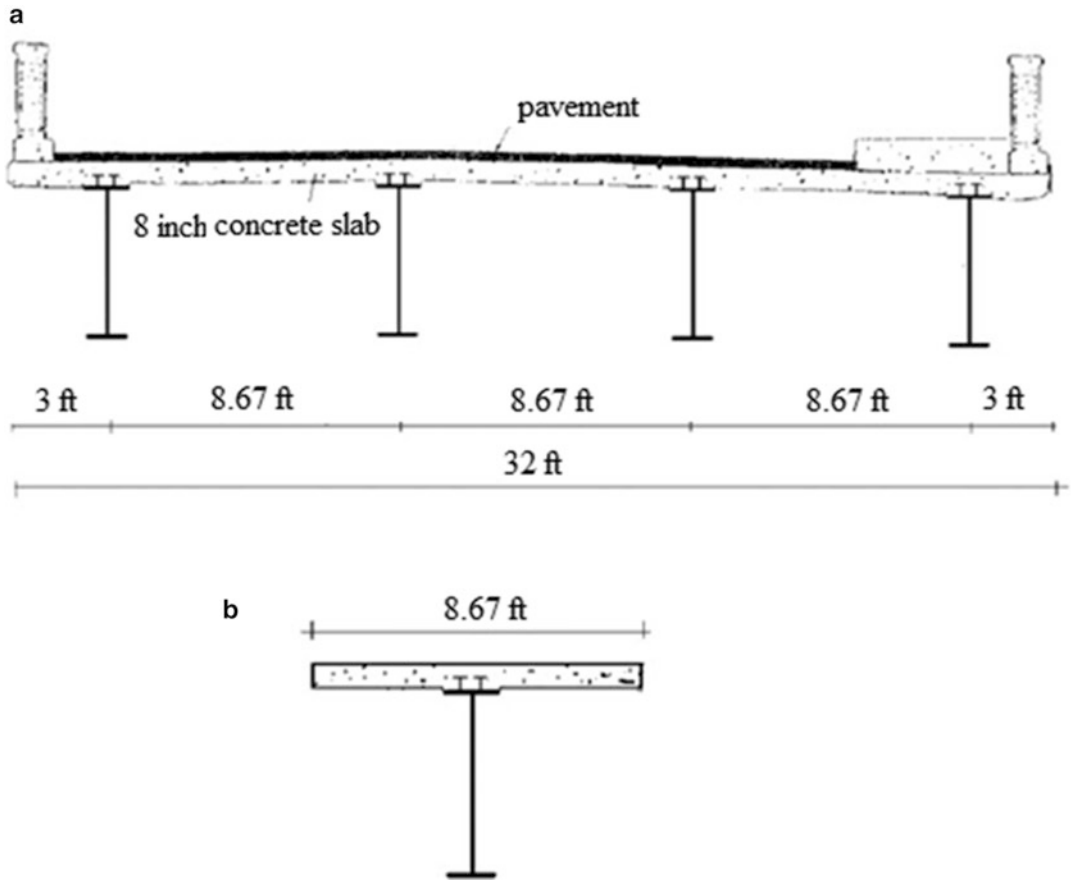


**Fig. 13.18** (**a**) Cross section—bridge deck. (**b**) Cross section of single composite beam

**Fig. 13.19** Truck load

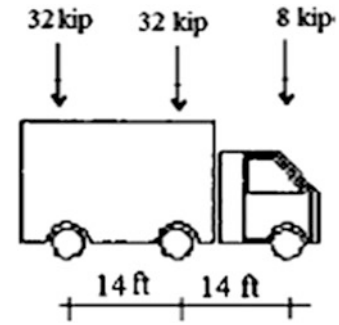


2. To establish the absolute peak values (positive and negative) for moment due to dead loading of 2.1 kip/ft, lane loading, and design truck loading.
3. To determine the moments due to: 1 in. settlement of support A; 1 in. settlement of support B.

*Loading patterns*:

The loading patterns for the uniform dead and lane loading are shown in Figs. 13.20 and 13.21.

We discretize the individual spans into ten segments, as indicated in Fig. 13.22. A computer software system is used to generate the solutions and the moment envelopes. One can assume an

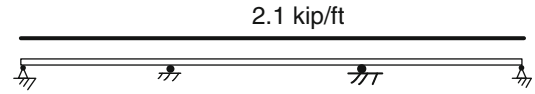


**Fig. 13.20** Uniform dead load pattern

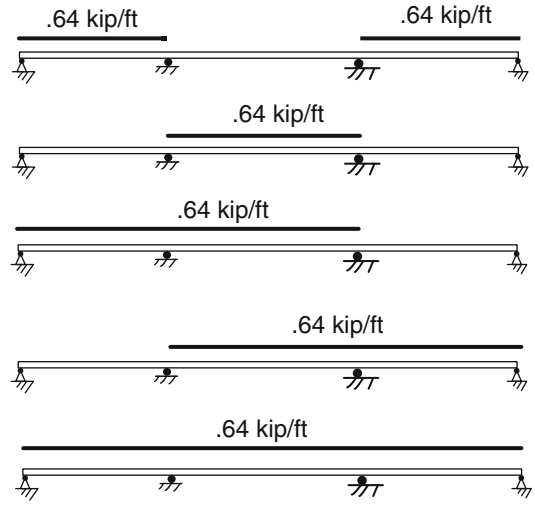


**Fig. 13.21** Uniform lane load patterns for positive and negative moments

arbitrary value for $I$ since the moment results are independent of $I$. Computer-based analysis is ideally suited for envelopes. Certain software packages have incorporated special features that automate the process of moving the load across the span and compiling the peak positive and negative moment values at each discrete section. Both the positive and negative moment envelopes are required in order to dimension the beam cross section.

*Dead load*:

The envelopes for dead load coincide with the actual moment and shear distribution shown below (Fig. 13.23). The peak values of shear, moment, and deflection are listed below.

$$\begin{cases} M^{-}_{\mathrm{DLmax}} = 1975\,\mathrm{kip\,ft} \\ M^{+}_{\mathrm{DLmax}} = 1202\,\mathrm{kip\,ft} \\ V_{\mathrm{DLmax}} = 115.5\,\mathrm{kip} \\ \delta_{\mathrm{DLmax}} = 1.1\,\mathrm{in.\,span\,II} \\ \delta_{\mathrm{DLmax}} = 1.26\,\mathrm{in.\,span\,I\,or\,III} \end{cases}$$

#### 13.4.1.1 Uniform Lane Load

The uniform load patterns defined in Fig. 13.21 are analyzed separately; based on this data, the following envelopes are generated (Fig. 13.24).

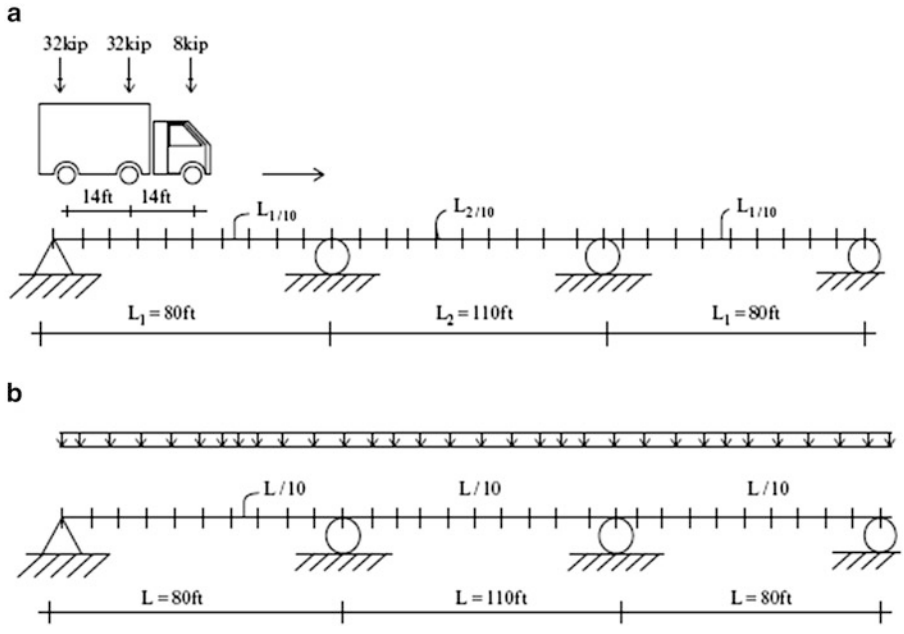


**Fig. 13.22** Span discretization for live loads. (**a**) Truck. (**b**) Lane load

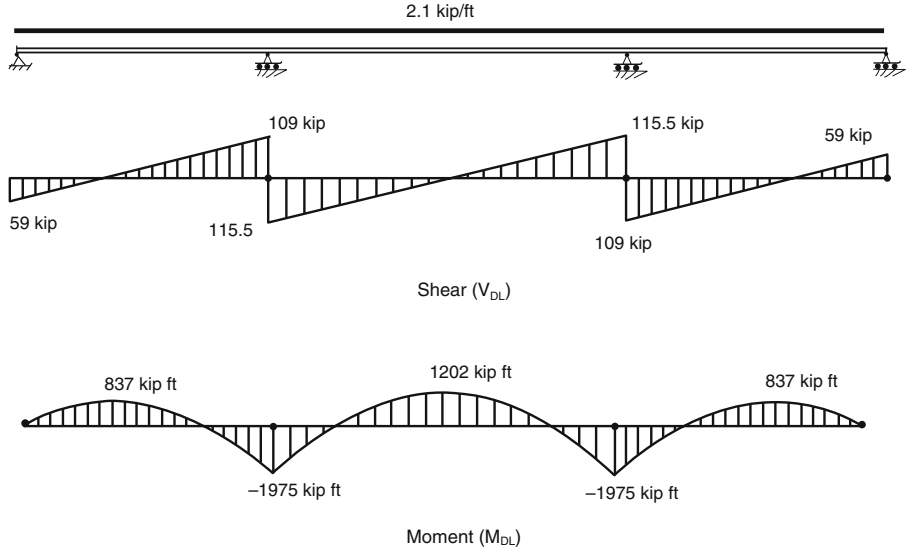


**Fig. 13.23** Dead load shear and moment distributions

### 13.4.1.2 Truck Loading

The truck loading defined in Fig. 13.22a is passed over the span leading to the envelopes plotted in Fig. 13.25. This moment needs to be modified to account for the distribution between adjacent

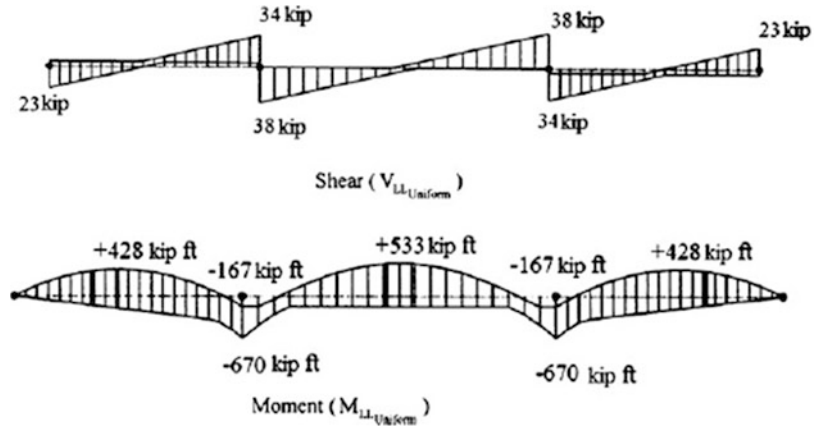


**Fig. 13.24** Uniform lane load envelopes

stringers and impact. The final values are determined using

$$\mathrm{DF} = \frac{1}{2}\left(2 - \frac{a}{S}\right) = \frac{1}{2}\left(2 - \frac{6}{8.67}\right) = 0.65$$

$$M_{\mathrm{Design}_{\mathrm{truck}}} = M_{\mathrm{LL}_{\mathrm{truck}}}(1 + I)\mathrm{DF} = M_{\mathrm{LL}_{\mathrm{truck}}} 1.3(0.65) = 0.845 M_{\mathrm{LL}_{\mathrm{truck}}}$$

Numerical results for the modified moment envelope values at the discrete points (interval of $L/10$) are listed in Tables 13.1, 13.2, and 13.3. Note that the results for span III are similar but not identical to the results for span I. Although the structure is symmetrical, the truck loading is not symmetrical.

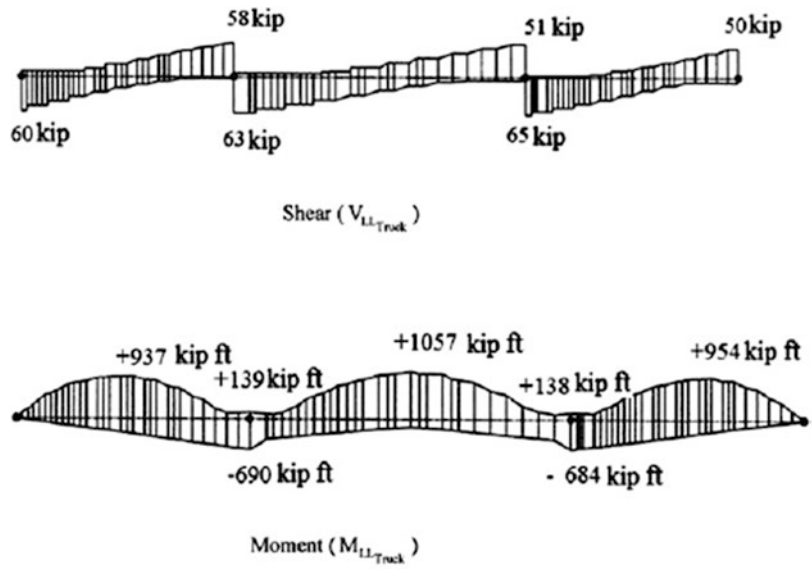


**Fig. 13.25** Truck loading envelopes

**Table 13.1** Discrete envelope values: Span I (kip ft)

| Span I | | | | | |
|---|---|---|---|---|---|
| $X$ | $M_{DL}$ | $M^{+}_{Design_{truck}}$ | $M^{-}_{Design_{truck}}$ | $M^{+}_{LL_{uniform}}$ | $M^{-}_{LL_{uniform}}$ |
| 0 | 0 | 0 | 0 | 0 | 0 |
| 0.1 $L$ | 407 | 344 | –58 | 168 | –43 |
| 0.2 $L$ | 680 | 576 | –117 | 294 | –87 |
| 0.3 $L$ | 819 | 703 | –175 | 380 | –130 |
| 0.4 $L$ | 823 | 775 | –233 | 425 | –174 |
| 0.5 $L$ | 693 | 792 | –292 | 428 | –217 |
| 0.6 $L$ | 428 | 718 | –350 | 391 | –261 |
| 0.7 $L$ | 29 | 568 | –408 | 313 | –304 |
| 0.8 $L$ | –504 | 357 | –466 | 194 | –348 |
| 0.9 $L$ | –1172 | 106 | –525 | 34 | –419 |
| $L$ | –1975 | 117 | –583 | – | –670 |

**Table 13.2** Discrete envelope values: Span II (kip ft)

| Span II | | | | | |
|---|---|---|---|---|---|
| $X$ | $M_{DL}$ | $M^{+}_{Design_{truck}}$ | $M^{-}_{Design_{truck}}$ | $M^{+}_{LL_{uniform}}$ | $M^{-}_{LL_{uniform}}$ |
| 0 | –1975 | 117 | –583 | – | –670 |
| 0.1 $L$ | –831 | 116 | –351 | – | –291 |
| 0.2 $L$ | 58 | 430 | –298 | 192 | –167 |
| 0.3 $L$ | 693 | 674 | –247 | 387 | –167 |
| 0.4 $L$ | 1074 | 823 | –194 | 495 | –167 |
| 0.5 $L$ | 1202 | 893 | –144 | 533 | –167 |
| 0.6 $L$ | 107 | 851 | –196 | 495 | –167 |
| 0.7 $L$ | 693 | 700 | –248 | 378 | –167 |
| 0.8 $L$ | 58 | 454 | –301 | 192 | –167 |
| 0.9 $L$ | –831 | 143 | –353 | – | –291 |
| $L$ | –1975 | 117 | –583 | – | –670 |

**Table 13.3** Discrete envelope values: Span III (kip ft)

| Span III | | | | | |
|---|---|---|---|---|---|
| $X$ | $M_{DL}$ | $M^{+}_{Design_{truck}}$ | $M^{-}_{Design_{truck}}$ | $M^{+}_{LL_{uniform}}$ | $M^{-}_{LL_{uniform}}$ |
| 0 | –1975 | 167 | −578 | – | −670 |
| 0.1 $L$ | –1172 | 105 | −520 | 34 | −419 |
| 0.2 $L$ | –504 | 330 | −462 | 194 | −348 |
| 0.3 $L$ | 29 | 532 | −405 | 313 | −304 |
| 0.4 $L$ | 428 | 682 | −346 | 391 | −261 |
| 0.5 $L$ | 693 | 777 | −289 | 428 | −217 |
| 0.6 $L$ | 823 | 806 | −232 | 425 | −174 |
| 0.7 $L$ | 819 | 742 | −173 | 380 | −130 |
| 0.8 $L$ | 680 | 575 | −116 | 294 | −130 |
| 0.9 $L$ | 407 | 334 | –57 | 168 | –43 |
| $L$ | 0 | 0 | 0 | 0 | 0 |

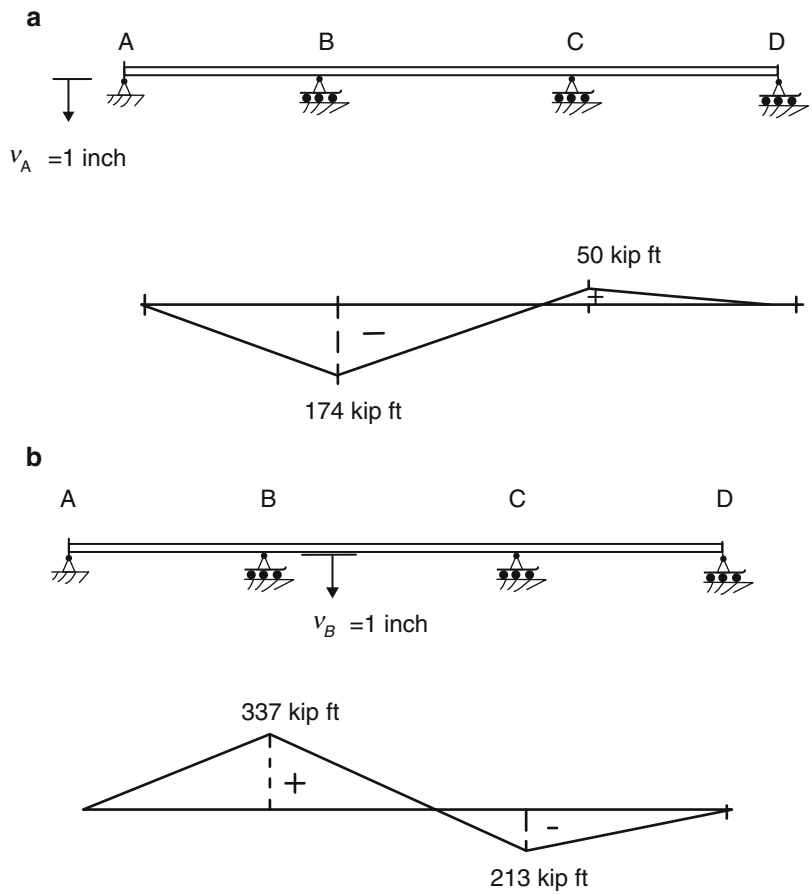


**Fig. 13.26** Moment due to support settlements ($E = 29{,}000$ ksi and $I = 48{,}110$ in.$^4$). (**a**) Settlement at A. (**b**) Settlement at B

#### 13.4.1.3 Support Settlement

We deal with support settlement by assuming a value for $EI$ (in this case, we take $E = 29{,}000$ ksi and $I = 48{,}110$ in.$^4$). Once the actual $EI$ is established, the moment results can be scaled. The corresponding moment diagrams are plotted in Fig. 13.26.

### 13.4.2 Case Study II: Two-Hinged Parabolic Arch Response—Truck Loading

This study illustrates how one evaluates the behavior of a typical two-hinged arch bridge subjected to a truck loading. An example structure is shown in Fig. 13.27; the idealized model is defined in Fig. 13.28. We model the roadway as a continuous longitudinal beam supported at 10 ft intervals by

**Fig. 13.27** Two-hinged arch bridge

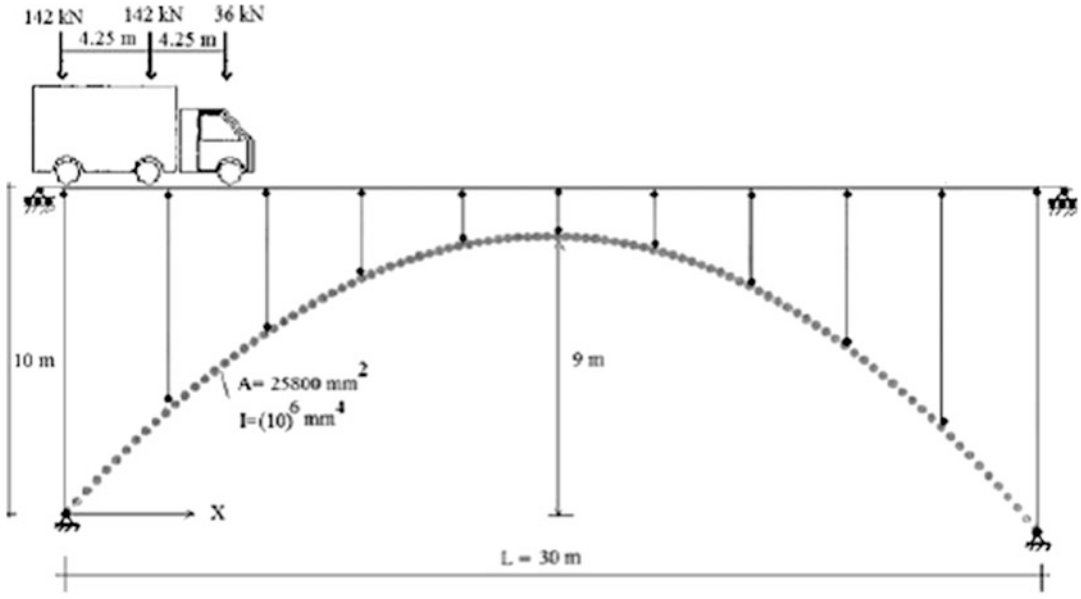


**Fig. 13.28** Parabolic-arch geometry and loading-idealized model

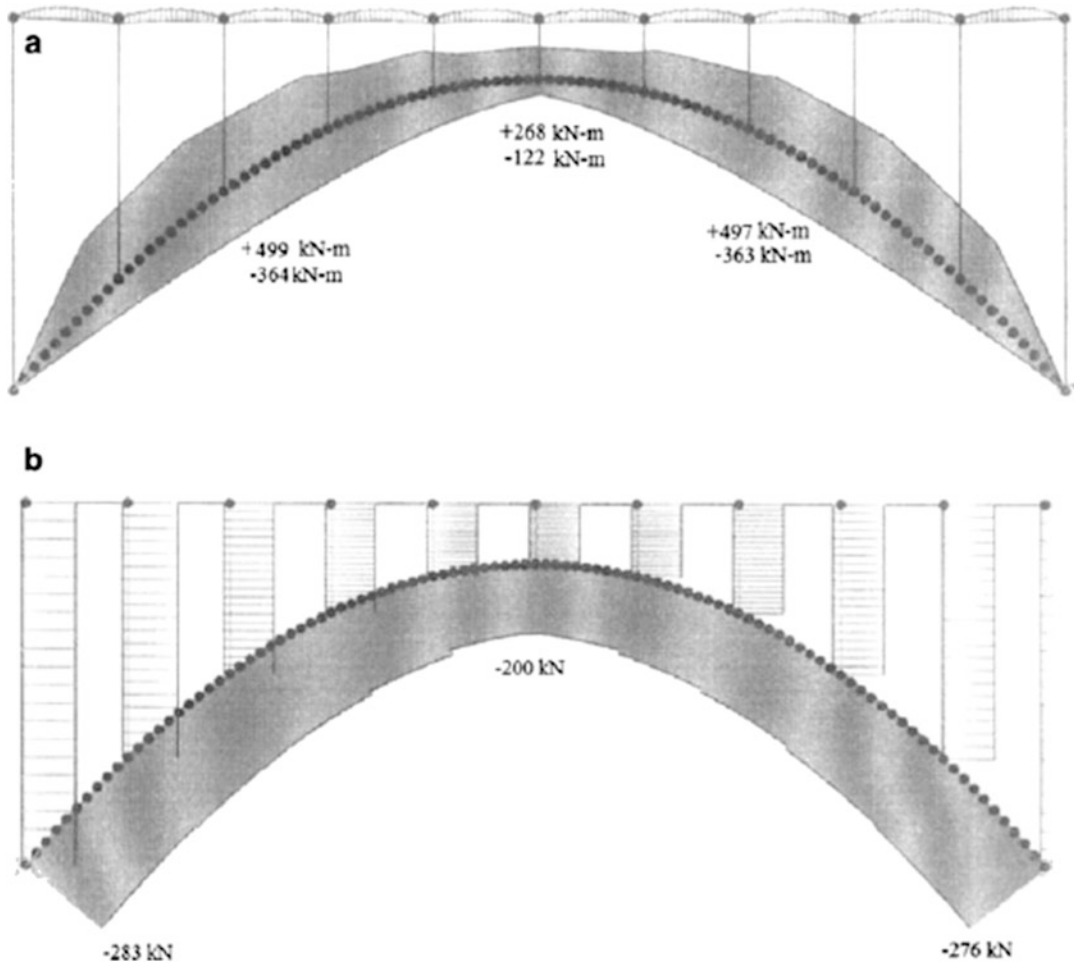


**Fig. 13.29** Force envelopes—Truck loading—100 straight segments. (**a**) Moment envelope. (**b**) Axial envelope

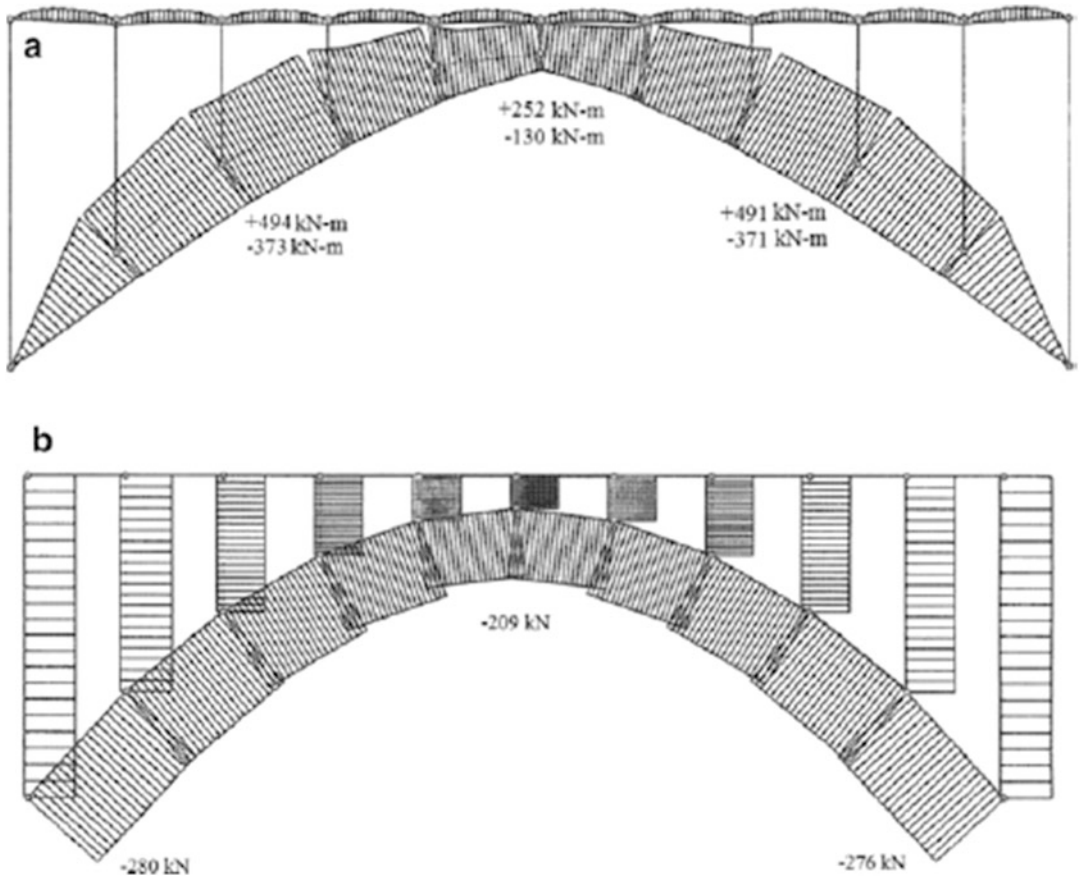


**Fig. 13.30** Force envelopes—Truck loading—10 straight segments. (**a**) Bending envelope. (**b**) Axial envelope

axial members attached to the parabolic arch. The truck loading is transmitted through the axial elements to the arch. We generate force envelopes for the arch using an analysis software system applied to the discretized model. A similar discretization strategy was employed in Chap. 6. Results for the bending moment and axial force due to the truck loading are plotted in Figs. 13.29 and 13.30. Figure 13.29 is obtained by subdividing the arch into 100 straight segments having a constant projection, $\Delta x$, of 0.3 m. Figure 13.30 is generated by subdividing the arch into ten straight segments having a constant projection, $\Delta x$, of 3 m.

The force envelope plots are useful for displaying the variation in response, e.g., the range in moment values. However, to determine the absolute extreme values, one has to scan over the data. This process leads to the following "absolute values"

$$100\,\text{straight segment}\begin{cases} M^{+}_{\max} = +499\,\text{kN m} \\ M^{-}_{\max} = -381\,\text{kN m} \\ P_{\max} = -283\,\text{kN} \end{cases} \qquad 10\,\text{straight segment}\begin{cases} M^{+}_{\max} = +499\,\text{kN m} \\ M^{-}_{\max} = -381\,\text{kN m} \\ P_{\max} = -283\,\text{kN} \end{cases}$$

In general, it is a good strategy to consider at least two discretizations. In this example, we observe that the ten segment model produces quite reasonable results.

### 13.4.3 Case Study III: Three-Span Parabolic Arch Response—Truck Loading

We consider next the three-span arch system shown in Fig. 13.31. The span lengths, discretizations, and the truck loading are the same as for case study I. It is of interest to compare the peak values of the force envelopes for the two different structural models. The discretized model consists of straight segments having a constant horizontal projection of 1 ft. A computer software package was used to generate the corresponding force envelopes which are plotted in Figs. 13.32 and 13.33.

Comparing the moment envelopes for the arch and the girder, we note that arch system has lower peak moment values. However, the arch system has axial forces so that the cross section must be designed for combined bending and axial action. There are no axial forces in the girder system, just pure bending.

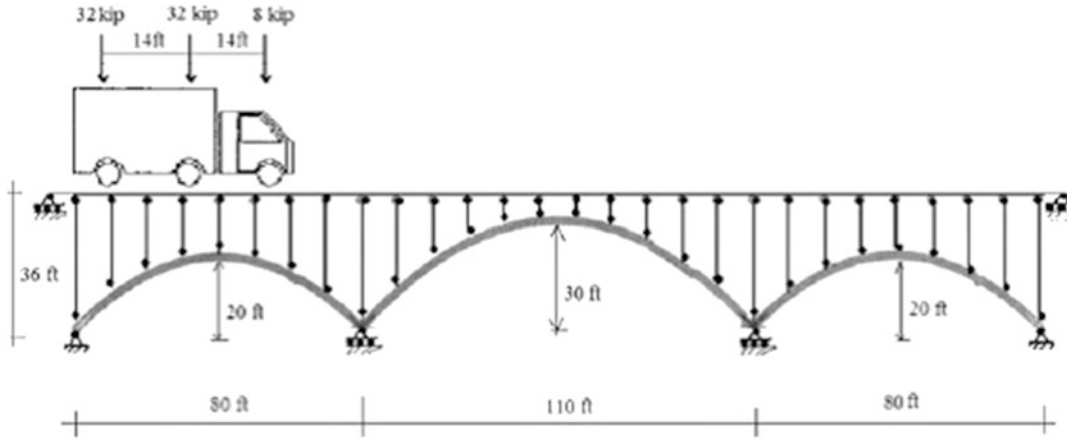


**Fig. 13.31** Idealized model—three-span arch

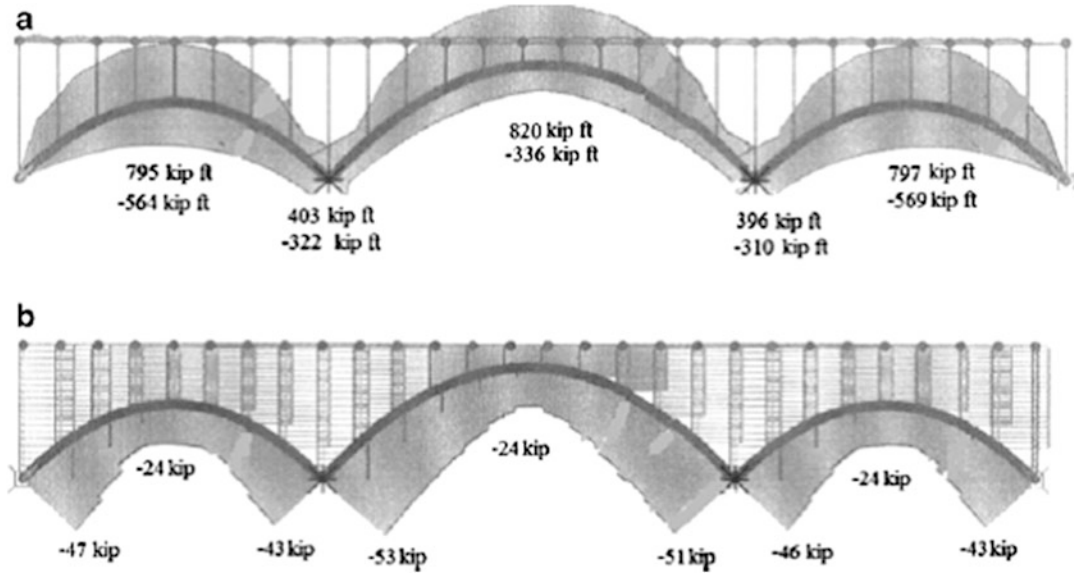


**Fig. 13.32** Force envelopes—three-span arch. (**a**) Moment envelope—three-span arch. (**b**) Axial envelope—three-span arch

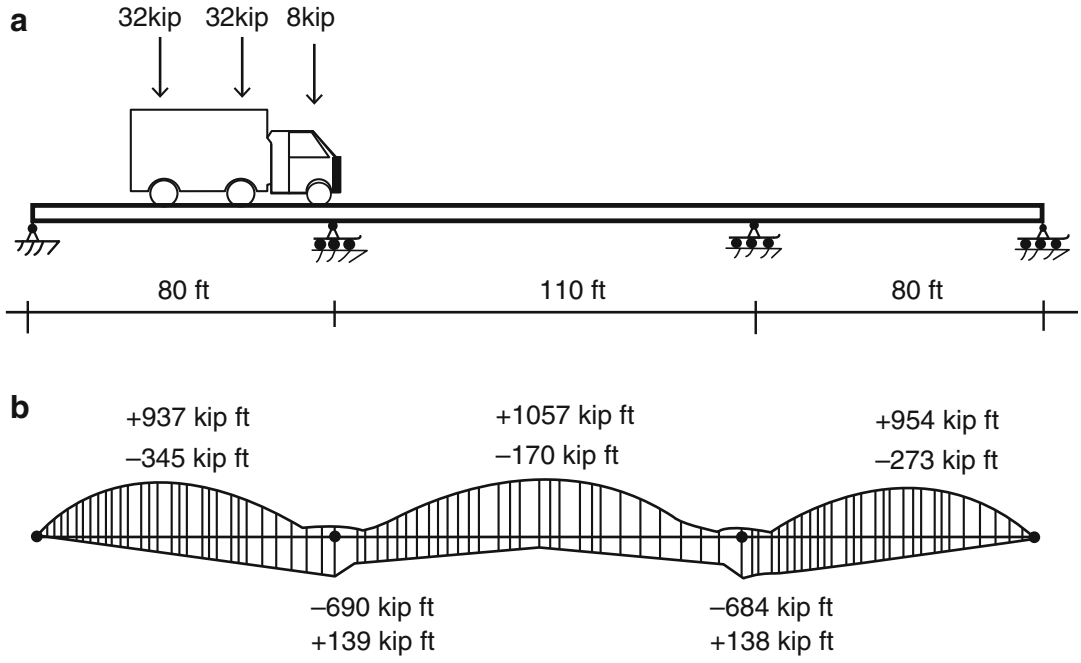


**Fig. 13.33** Force envelopes—three-span girder. (**a**) Geometry and loading. (**b**) Moment envelope

### 13.4.4 Case Study IV: Cable-Stayed Bridge

This case study concerns the cable-stayed bridge concept, a type of structure that requires some special modeling strategies and exhibits a completely different behavioral pattern than girder and arch-type structures. It has evolved as the dominant choice for long span crossings. A typical configuration is shown in Fig. 13.34. The terms "harp" and "fan" refer to the positioning of the cables on the tower. A modified fan arrangement is usually adopted to avoid congestion on the tower.

**Fig. 13.34** Typical cable-stayed scheme

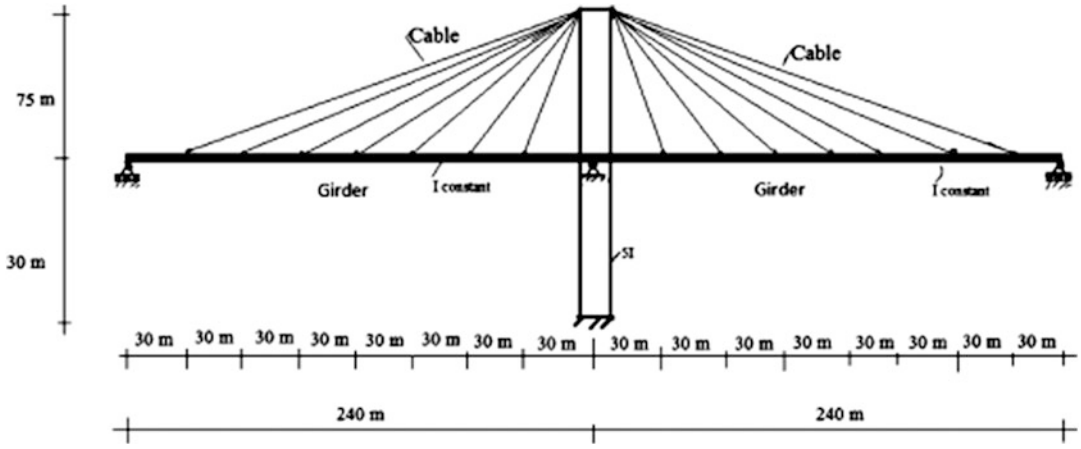


**Fig. 13.35** Idealized cable-stayed scheme

Of particular interest is the load path for vertical loading applied to the girder. Without the cables, the girder carries the load by bending action throughout the total span. Since the maximum moment varies as to the square of the span length, this structural concept is not feasible for long spans. The effect of the cables is to provide a set of vertical supports to the girder, thus reducing the moment in the girder. In what follows, we illustrate this effect using the idealized structure shown in Fig. 13.35.

We suppose the girder is continuous, and the cable layout is symmetrical (equally spaced on the longitudinal axis). There are seven pairs of symmetrical cables. Each cable has a different cross-sectional area. The girder is hinged at the tower, but free to expand at the two end supports. We model the cables as straight members that are hinged at their ends to the tower and the girder. In this way, they function as axial elements and transmit the gravity loading applied to the girder up to the tower. The net effect is to reduce the bending moment in the girder.

Starting with nodes at the supports and the cable–girder intersection points, one may also discretize the girder between the cable nodes to obtain more refined displacement and moment profiles. Since the structure is indeterminate, we need to specify member properties in order to execute an analysis. We estimate the cable areas by assuming an individual cable carries the tributary loading on a segment adjacent to the cable. This estimate is based on strength.

$$A_C = \frac{T}{\sigma_{all}} = \frac{w\Delta L}{\sigma_{all} \sin\theta}$$

where $\sigma_{all}$ is some fraction of the yield stress and $\Delta L$ is the cable spacing. This equation shows that the required area increases with decreasing $\theta$. Therefore, one must increase the cable area as the distance from the tower increases. A lower limit on $\theta$ is usually taken as 15° (Fig. 13.36).

Taking $w = 10$ kN/m, $\Delta L = 30$ m, and $\sigma_{all} = 0.687$ kN/mm$^2$ leads to the estimated cable areas listed below.

| Cable | $\theta$ ° | $\frac{1}{\sin\theta}$ | $A_{cable}$ (mm$^2$) |
|---|---|---|---|
| C1 | 19.6 | 3 | 1305 |
| C2 | 22.6 | 2.3 | 1130 |
| C3 | 26.5 | 2.2 | 957 |
| C4 | 32 | 1.9 | 827 |
| C5 | 39.8 | 1.6 | 696 |
| C6 | 51.3 | 1.3 | 566 |
| C7 | 68.2 | 1.1 | 480 |

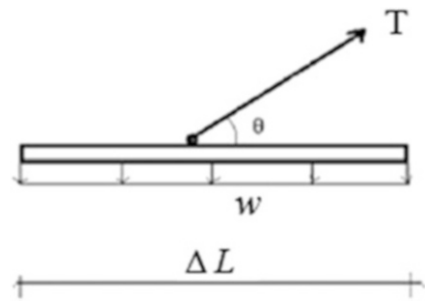


**Fig. 13.36** Tributary area for cable

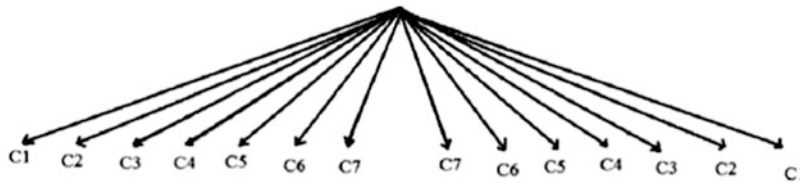


We estimate $I$ for the girder by assuming the bending moment diagram is similar to the distribution for a uniformly loaded beam with multiple spans equal to $\Delta L$. The peak negative moment for this case is $\frac{w(\Delta L)^2}{12}$. Given these estimated properties, one analyzes the structure and iterates on the properties until the design requirements are satisfied.

Figure 13.37 shows the forces and displacement profile corresponding to $I_{\text{girder}} = 420(10)^6$ mm$^4$ and the following set of cable areas for cables 1–7, respectively (1305, 1130, 957, 827, 696, 566, and 480 mm$^2$). The girder cross-sectional area is taken as 120,000 mm$^2$. Note that the bending moment diagram for the girder is similar to that observed for a multi-span uniformly loaded beam. We also point out that the response is sensitive to the girder cross-sectional area since there is significant compression in the girder.

An estimate of the vertical displacement based on the axial force corresponding to strength is given by

$$v = \frac{\sigma L_{\text{cable}}}{E \sin\theta}$$

The displacement profile for the girder agrees with this approximation. The peak value occurs for the outermost cable which has the largest length and smallest angle.

A suggested peak value for displacement under live load is $L/800$, which for this geometry translates to 300 mm. We can decrease the deflection by increasing the areas for the outer cables. Assuming an individual cable act as a single vertical spring subjected to the loading $w(\Delta L)$, and requiring the displacement to be equal to $v_{\text{all}}$ leads to the following estimate for the cable area

$$A_{\text{c}} = \frac{w(\Delta L)L_{\text{c}}}{v_{\text{all}} E(\sin\theta)^2}$$

where $L_{\text{c}}$ is the cable length. Holding the girder properties constant, we use this approximate expression to increase the cable areas to (14,000, 11,500, 8500, 5000, 3000, 3000, 2000 mm$^2$) and repeat the analysis. The displacement profile of the girder for this case is plotted in Fig. 13.38 and also summarized in the table listed below. Note that the displacement is sensitive to the cable area and the angle of inclination; the cable tension is governed primarily by strength. This case study illustrates the

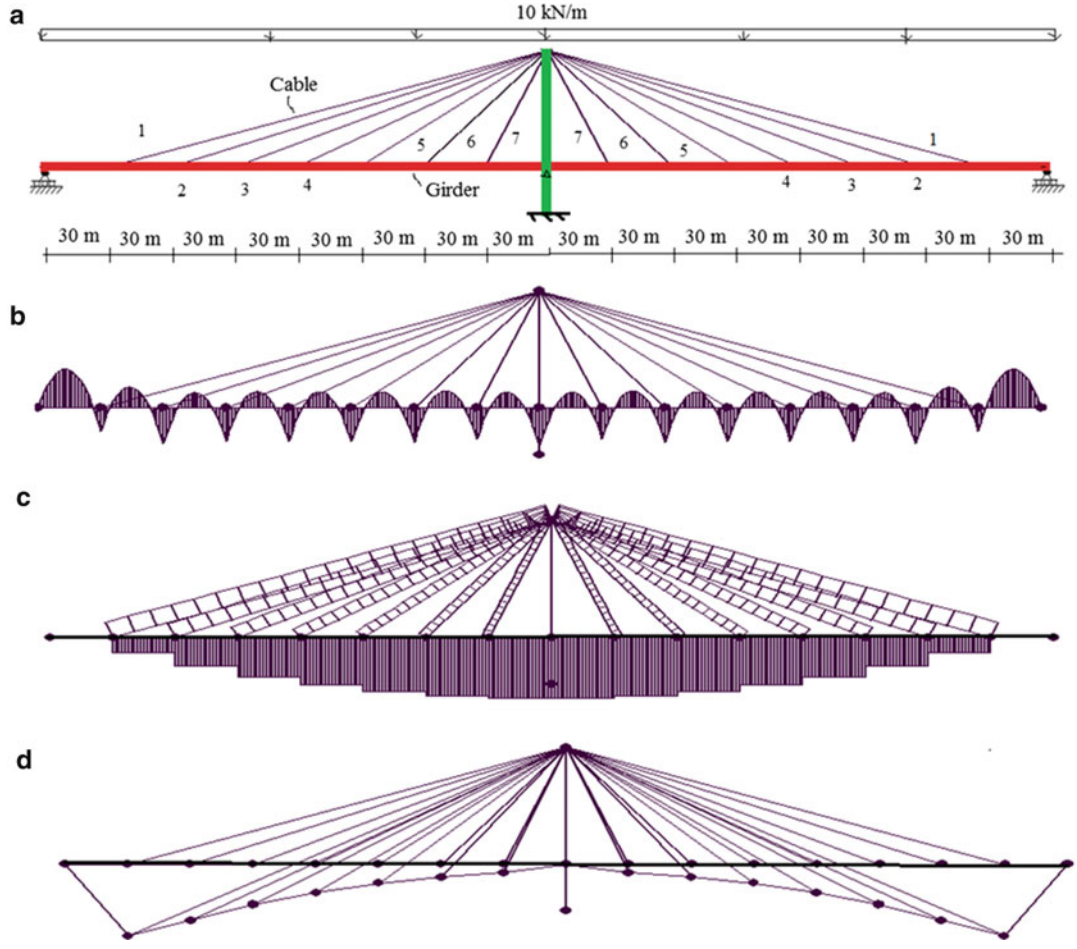


**Fig. 13.37** Force and displacement profiles. (**a**) Geometry and loading. (**b**) Moment in girder. (**c**) Axial forces in cables and girder. (**d**) Displacement profile of girder

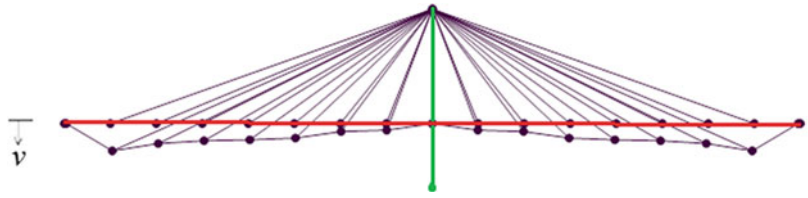


**Fig. 13.38** Final displacement profile of girder

role of computer simulation in developing the design of cable-stayed structures. One refines the design through iteration. This example also illustrates how cable-stayed structures carry the load primarily through axial action in the cables. The girder functions mainly to transmit the deck loading to the cables, i.e., the bending is localized between the cable support points.

| Cable | $A_{cable}$ (mm$^2$) | Tension (kN) | $v\downarrow$ (mm) | $A_{cable}$ (mm$^2$) | Tension (kN) | $v\downarrow$ (mm) |
|---|---|---|---|---|---|---|
| C1 | 1305 | 914 | 2382 | 14,000 | 998 | 297 |
| C2 | 1130 | 810 | 1864 | 11,500 | 761 | 217 |
| C3 | 957 | 665 | 1341 | 8500 | 675 | 186 |
| C4 | 827 | 567 | 940 | 5000 | 566 | 176 |
| C5 | 696 | 467 | 630 | 3000 | 467 | 157 |
| C6 | 566 | 387 | 428 | 3000 | 386 | 86 |
| C7 | 480 | 315 | 287 | 3000 | 386 | 48 |

## 13.5 Summary

### 13.5.1 Objectives

- To present Müller-Breslau's principle and illustrate how it is used to establish loading patterns that produce the maximum value of a force quantity at a particular point on a structure.
- To describe a procedure for determining the load on an individual stringer due to an axle load applied to the deck of a slab-stringer bridge system.
- To describe and illustrate a computer-based procedure for generating force envelopes for indeterminate horizontal structures subjected to a set of concentrated loads.
- To illustrate the different behavioral patterns for multi-span girder, arch, and cable-stayed systems.

### 13.5.2 Key Facts and Concepts

- Müller-Breslau's principle is used to establish influence lines for indeterminate structures. One works with a structure generated by removing the constraint provided by the force quantity. The deflected shape of the structure due to a unit value of the force quantity is a scaled version of the influence line.
- The moment envelope for a horizontal structure is generated by applying the loading at discrete points on the longitudinal axes, tabulating the bending moment at each discrete point for *all the loading cases*, and selecting the largest positive and negative values. A computer-based procedure is used for this task.
- Support settlement can produce bending moments which are significant for short span bridges.

## 13.6 Problems

**Problem 13.1**

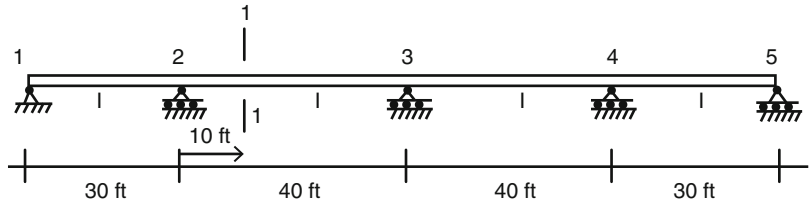


(a) Using Müller-Breslau principle, sketch the influence lines for the vertical upward reaction at support 3 ($R_3$), the negative moment at support 2 ($M_2$), and the negative moment at section 1-1 ($M_{1-1}$)

(b) Use a software package to determine:
   (i) The maximum values of $R_3$, $M_2$, and $M_{1-1}$ cause by a uniformly distributed dead load of 2 kip/ft.
   (ii) The maximum value of $M_2$ caused by a uniformly distributed live load of 1 kip/ft.

**Problem 13.2** Consider the single span bridge shown below. Using the analytical procedure described in Sect. 3.10.2.1, determine the absolute maximum value of moment developed as the truck loading defined below passes over the span. Repeat the analysis using computer software.

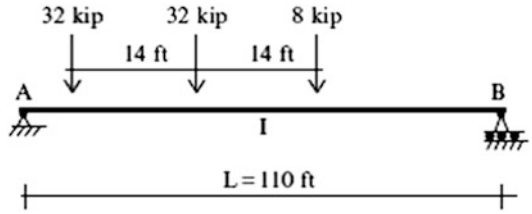


**Problem 13.3** Consider the two-span bridges shown below. Use computer software to determine global moment envelopes for both the lane and truck loadings defined below.

Lane load: $w = 10$ kN/m uniform

Truck load:

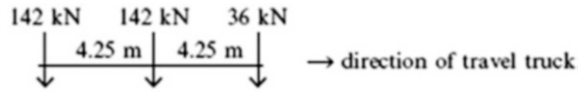


(a) $L_1 = L_2 = 30$ m, $EI$ is constant

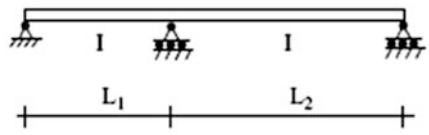

(b) $L_1 = 15$ m, $L_2 = 30$ m, $EI$ is constant

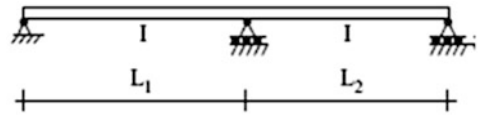


(c) $L_1 = L_2 = 30$ m, $EI$ is constant

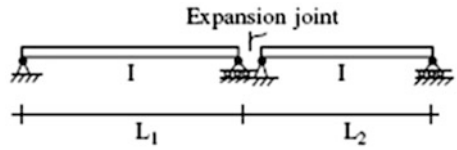


(d) Compare the global moment envelopes for the structure shown below with the envelopes generated in part (a). Is there any effect of varying $I$?

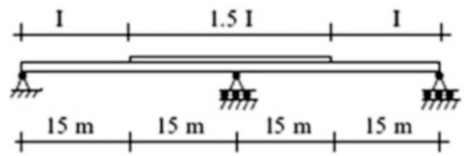


**Problem 13.4** Consider the multi-span bridge shown below. Suppose the bridge is expected to experience a temperature change of $\Delta T$ over its entire length. Where would you place a hinge support: at A or at B? Determine the end movement corresponding to your choice of support location.

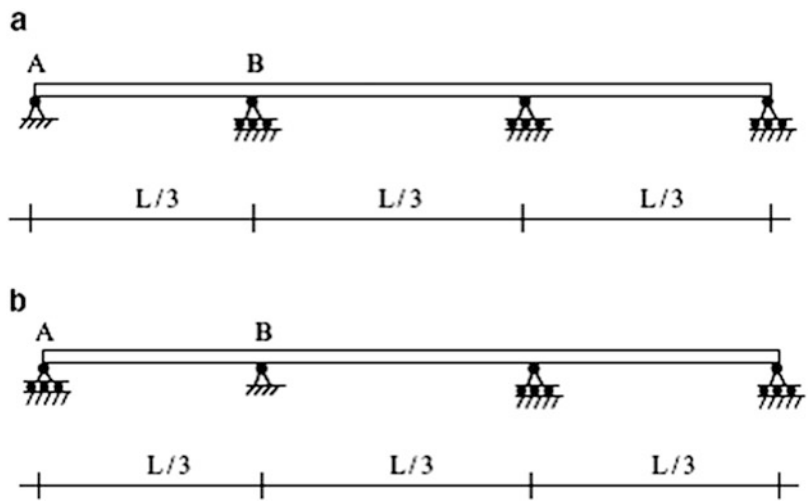

**Problem 13.5** Most design codes limit the deflection due to live loading to some fraction of length, say $L/\alpha$, where $\alpha$ is on the order of 500. Generate the global "deflection" envelope for the multi-span beam and truck loading shown below. Take $E = 29{,}000$ ksi and $I = 60{,}000$ in.$^4$

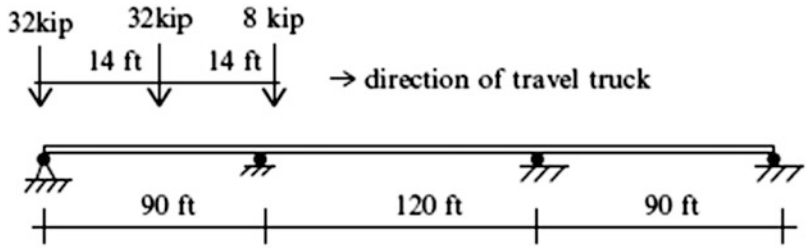


**Problem 13.6** Investigate convergence of the internal forces for the parabolic arch shown as the discretization is refined. Take the interval as 2.4, 1.2, and 0.6 m.

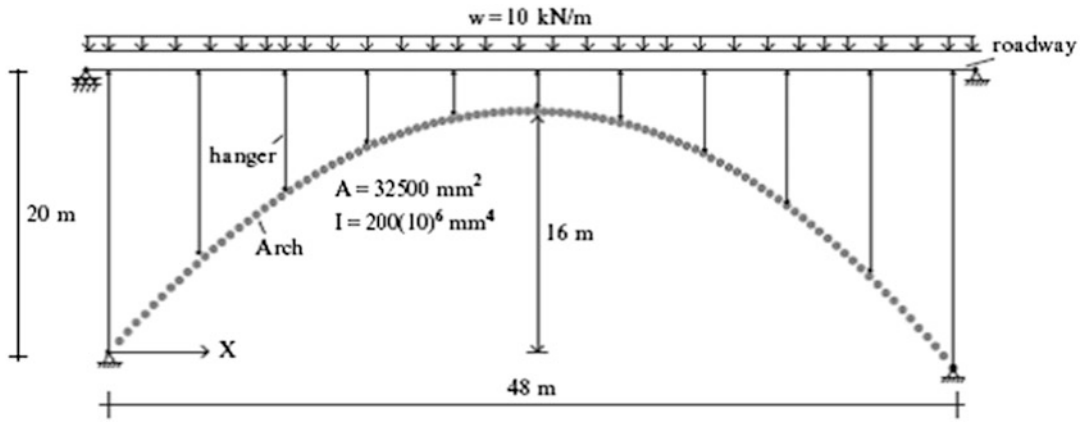


**Problem 13.7** Suppose a uniform loading is applied to span ABC. Investigate how the response changes as $x$ varies from $L/2$ to $L$. Take $h = L/2$, $A = 50$ in.$^2$, $A_C = 2$ in.$^2$, $w = 1$ kip/ft, $f = 1 + (2x/L)^2$.

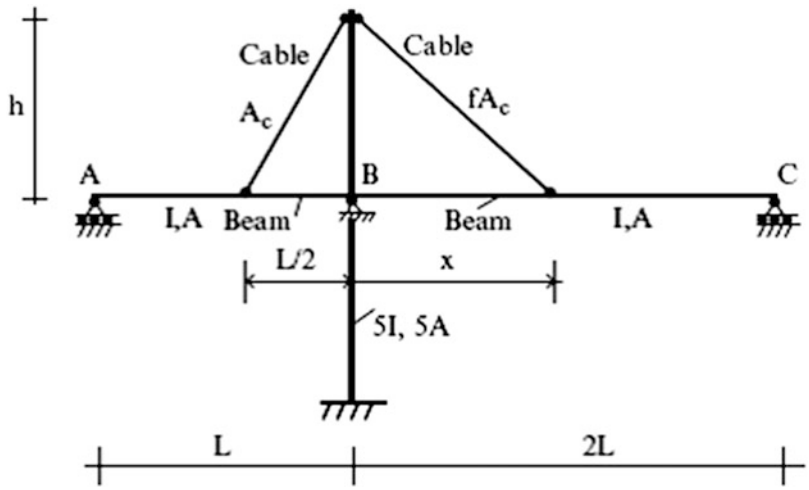

**Problem 13.8** Determine the structural response (forces and displacements) of the idealized tied arch shown below under a uniformly distributed gravity load of 30 kN/m.

Assume $A_{arch} = 26{,}000\ mm^2$, $I_{Arch} = 160(10)^6\ mm^4$, $A_{hanger} = 2(10)^6\ mm^2$

Note: roadway girder and arch are pinned together at points A and B.

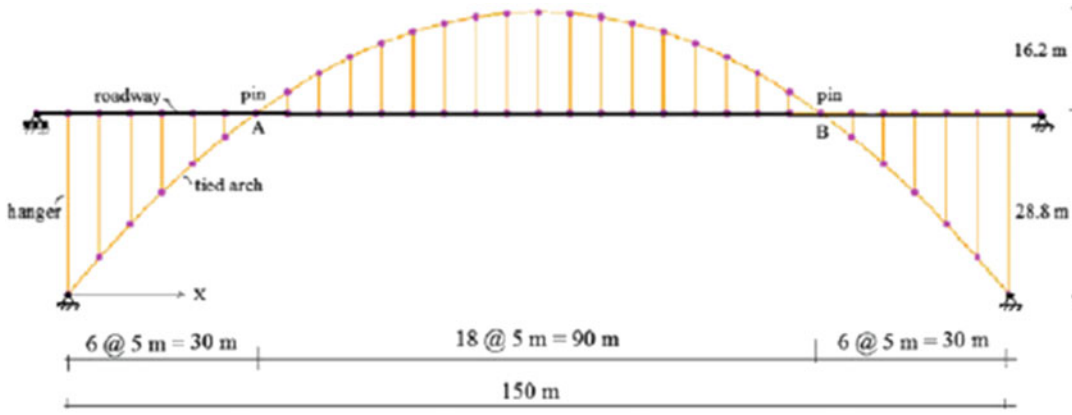


An actual structure is shown below.

**Problem 13.9** Determine the distribution of internal forces and displacements for the cable-stayed structure shown below. Member AB acts as counterweight for loading applied on member BC. The two members are connected by nine parallel equally spaced cables. Self-weight of members AB and BC is 16 and 8 kN/m, respectively. Assume $A_{Cable} = 50{,}000\ mm^2$ and $E = 200$ GPa. Consider the following cases:

(a) $I_{AB} = I_{BC} = 40(10)^9\ mm^4$

(b) $I_{AB} = 4I_{BC}\ I_{BC} = 40(10)^9\ mm^4$

(c) Uniform live load of 2 kN/m applied to member BC in addition to self-weight.
$I_{AB} = 4I_{BC}\ I_{BC} = 40(10)^9\ mm^4$

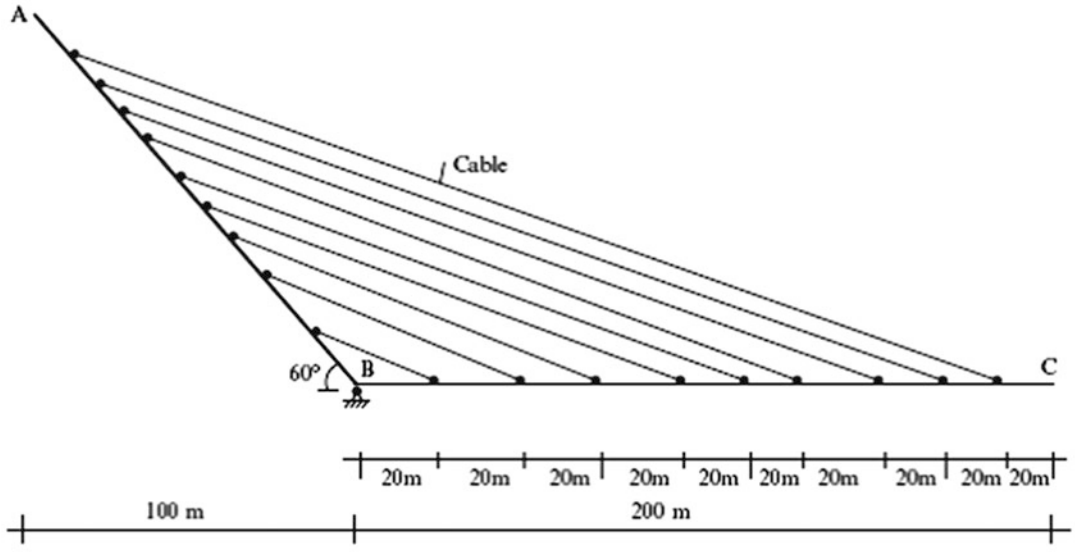


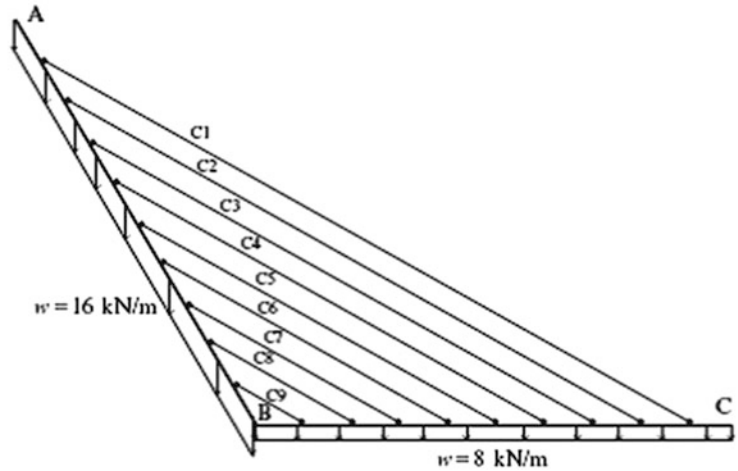


An illustration of this structural concept created by Santiago Calatrava is shown below. This bridge is located in Seville, Spain. Puente del Alamillo in Seville, Spain. This work has been released into the public domain by its author, Consorcio Turismo Sevilla. This applies worldwide. The image was accessed in March 2012 from http://en.wikipedia.org/wiki/File:Puente_del_Alamillo.jpg.

**Problem 13.10** Consider the symmetrical cable structure shown below. Determine a set of cable areas ($C_1$–$C_{10}$) such that the maximum vertical displacement is less than 375 mm under a uniformly distributed live load of 10 kN/m. Assume $I_{\text{girder}} = 400(10)^6$ mm$^4$, $A_{\text{girder}} = 120(10)^3$ mm$^2$. Take the allowable stress as 700 MPa.

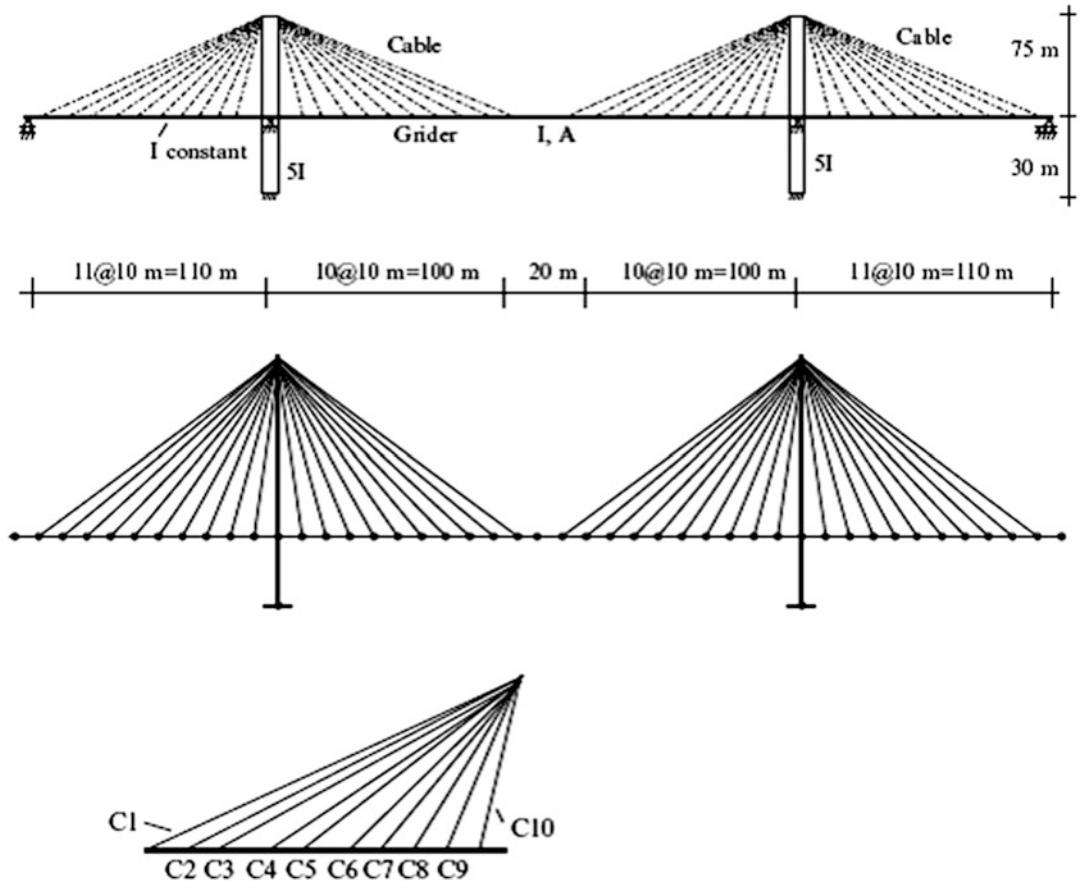


## References

1. Wilbur JB, Noris CH. Elementary structural analysis. New York: McGraw-Hill; 1948.
2. Faraji S, Ting J, Crovo DS, Ernst H. Nonlinear analysis of integral bridges: finite element model. ASCE J Geotech Geoenviron Eng. 2001;127(5):454–61.